Colloquium: An algebraic model of localized surface plasmons and their interactions

T. J. Davis

School of Physics, University of Melbourne, Parkville Victoria Australia

D. E. Gómez

Centre of Excellence for Exciton Science, RMIT University, Melbourne, 3000, Australia

(published 30 January 2017)

Although localized surface plasmons in metal nanoparticles can be modeled by Maxwells equations, the difficulty in solving them forces many researchers to use numerical methods. Such methods give accurate results but rarely provide much insight into the complex behaviors of the surface plasmons, nor do they provide a means to choose a configuration of metal nanoparticles to achieve a desired optical response. This Colloquium presents a simple algebraic approach for modeling localized surface plasmons, their excitation by light, and their interactions with one another. Although the method is not numerically accurate it yields useful insight into plasmon behavior and provides a basis for the design of complex plasmonic devices. The approach relies on a description of the surface plasmons in terms of a set of eigenmodes. However, the functional form of these modes is not usually required and the entire problem is reduced to a simple algebra involving the plasmon amplitudes, resonance terms, and their mutual coupling. The algebraic method is derived from an electrostatic formalism, appropriate for near-field interactions at optical frequencies, which is then used to demonstrate a variety of optical effects associated with localized surface plasmons, such as plasmon hybridization, induced transparency, Fano resonances, optical phase detection, and all-optical modulation, among others.

DOI: 10.1103/RevModPhys.89.011003

CONTENTS

I. Introduction 1
II. A Theory of Localized Surface Plasmon Resonances 2
A. The electrostatic eigenvalue problem 3
B. LSP excitation amplitudes 5
C. Optical theorem, energy conservation, and radiation 6
1. Absorption 6
2. Radiation 7
3. Radiation damping 7
D. Properties of isolated metal nanostructures 8
1. An example with multiple LSP resonances 8
E. Coupled LSPs 9
III. Analyzing Interactions between Coupled LSPs 10
A. Two particle coupling, dark modes, and Fano resonances 10
1. Plasmon hybridization 11
2. Bright and dark modes 12
3. Fano resonances 12
B. Coupling in three nanorod structures 12
1. Plasmon-induced transparency 13
2. Plasmonic Wheatstone bridge 13
3. All-optical modulation 14
4. Radially symmetric structures and dark modes 15
C. Coupling in 3D structures 16
IV. Concluding Remarks 17
Acknowledgments 17
Appendix A: The Eigenmodes and Eigenvalues of Eq. (4) for a Sphere 17
Appendix B: Drude Model and the Electrostatic Approximation 18
References 19

I. INTRODUCTION

Localized surface plasmons (LSPs) are oscillations of the conduction electrons excited by light on the surfaces of metal nanoparticles (Raether, 1977, 1988; Kreibig and Vollmer, 1995; Barnes, Dereux, and Ebbesen, 2003; Zayats, Smolyaninov, and Maradudin, 2005; Ozbay, 2006; Maier, 2007; Odom and Schatz, 2011). There has been great interest in LSPs among scientists and engineers, due in part to their properties such as confining light to nanoscale volumes (Bozhevolnyi *et al.*, 2006), enabling light energy and spectral content to be manipulated (Kim *et al.*, 1999; Li, Butun, and Aydin, 2014), preserving phase coherence (Fakonas *et al.*, 2014), and quantum coherence (Chang *et al.*, 2006). By placing metal nanoparticles in closed proximity the LSPs couple through their evanescent electric fields, which alters their resonance properties enabling unusual optical effects, such as plasmon "induced" transparency (Zhang *et al.*, 2008; Liu *et al.*, 2009; Hokari, Kanamori, and Hane, 2014), suppressed light scattering (dark modes), and Fano resonances (Fano, 1961; Mirin, Bao, and Nordlander, 2009; Luk'yanchuk *et al.*, 2010; Miroshnichenko, Flach, and Kivshar, 2010), among others. These properties depend on the geometry

and composition of the metal nanoparticles, their dielectric environment, and also on their mutual interactions. The problem is to understand how the complex interplay between these parameters modifies the optical properties of the nanoparticles and how one can design a configuration of coupled metal nanoparticles to achieve a desired optical effect.

There are many methods that can be used to model the interaction of light with LSPs, ranging from simple coupled oscillator models (Zhang *et al.*, 2008; Liu *et al.*, 2009; Taubert *et al.*, 2012; Lovera *et al.*, 2013) to full analytical and numerical solutions to Maxwell's equations including (but not limited to) the finite-difference time-domain (FDTD) method (Taflove *et al.*, 2000), a rigorous coupled wave analysis (Moharam *et al.*, 1995; Lalanne and Morris, 1996; Lalanne and Jurek, 1998; Weiss *et al.*, 2009), the discrete dipole approximation (Draine and Flatau, 2003; Yurkin and Hoekstra, 2007), and the boundary element method (García de Abajo and Howie, 2002; Hohenester and Krenn, 2005). However, in our view none of these methods provide a simple means for understanding how the physical parameters affect a given optical response of an ensemble of metal nanostructures.

The aim of this Colloquium is twofold. First we present a physical description of coupled LSPs, based on an expansion in terms of eigenmodes (or fundamental resonances), that enables the rational design of complex plasmonic structures without the need for time and resource consuming numerical calculations. Second, we use this algebraic model to describe some of the important experimental observations that arise from localized surface plasmon resonance phenomena. The model is constructed using approximate forms of Maxwell equations that neglect retardation and higher-order electric-magnetic coupling, and consequently cannot accurately predict quantitatively measured experimental properties such as resonance frequencies and linewidths. The strength of the approach is the *algebraic relationships* between the physical parameters that predict experimentally observable optical effects, which provides insight into LSPs and their interactions and guides us to the underlying physics.

The outline of this Colloquium is as follows. In Sec. II we develop the theory of LSPs based on an "electrostatic" approximation that leads to a physical description of resonances in terms of *eigenmodes*. The expansion coefficients, or LSP excitation amplitudes, become the key element in the algebraic model and we use these amplitudes to present some of the properties of LSPs in single metal nanostructures. The model is then supplemented with an equation describing the coupling between LSPs mediated by their electric near fields. In Sec. III we apply this algebraic model to important experimental observations that arise from localized surface plasmon resonance phenomena.

II. A THEORY OF LOCALIZED SURFACE PLASMON RESONANCES

Localized surface plasmons excited by light on metal nanoparticle surfaces are observed experimentally by strong scattering at a particular frequency—the resonance frequency of the LSP. Such resonances have been known for a long time. In spherical metal nanoparticles (Mie, 1908) these are known as Fröhlich resonances (Bohren and Huffman, 1983) and are the fundamental electric dipole resonances of spheres.

So how do the resonances come about and how can we model them mathematically? What happens when two or more metal particles are close to one another and their resonating electric fields overlap?

The surface plasmons are well described by classical electromagnetism embodied in Maxwell's equations. One of the simplest cases is a semi-infinite metal-dielectric interface (Raether, 1977, 1988). If we consider an electromagnetic wave at the interface and seek a solution involving outwardly propagating waves only, we find a wave traveling along the interface with a wave number $\alpha = k[\epsilon_m\epsilon_b/(\epsilon_m+\epsilon_b)]^{1/2}$, where ϵ_m and ϵ_b are the respective electric permittivities of the metal and the dielectric, and $k=\omega/c$ is the free-space wave number. At visible and infrared frequencies, the real part of the electric permittivity of a metal is negative $\mathrm{Re}\epsilon_m < 0$ and large $|\epsilon_m| \gg \epsilon_b$ which means that α is complex and larger than the free-space wave vector ($|\alpha| > k$). Such a wave cannot radiate into free space and is therefore trapped at the metal surface. This wave is a *surface plasmon polariton*—a wave of surface charge propagating over the metal surface (Raether, 1977; Maier, 2007) coupled with its electromagnetic field in the adjacent dielectric medium. The electric field is strong at the surface but decays exponentially with distance into the metal and into the adjacent dielectric medium. This decaying field is known as an *evanescent* wave.

The surface plasmon wave reflects from discontinuities, such as a dielectric ridge or a defect in the metal surface (Zayats, Smolyaninov, and Maradudin, 2005). If the film contains multiple boundaries, a surface plasmon standing wave can arise at certain frequencies where the multiple reflections overlap in phase (Schouten *et al.*, 2005; Pacifici, Lezec, and Atwater, 2007). If we now think of surface plasmon waves propagating over the surface of a metal particle, the waves travel around the surface, overlap, and interfere. When the path length is an integer number of surface plasmon wavelengths, constructive interference occurs and a standing wave is formed. This condition occurs only at specific frequencies of the incident light: these standing waves are the localized surface plasmon resonances.

Although Maxwell's equations can describe the LSPs, the analytical solutions for arbitrarily shaped metal nanoparticles are unavailable in closed form and the equations require numerical evaluation (Mäkitalo, Kauranen, and Suuriniemi, 2014). Solutions describing the resonances arise from complicated eigenvalue problems, where the eigenvalues depend in a nonlinear fashion on the frequency. One of the problems relates to the interaction between the time-varying electric and magnetic fields. The surface plasmons are excited by the incident electric fields that oscillate in time producing oscillating magnetic fields. The oscillating magnetic fields react back on the charges, inducing displacement currents (Faraday's law) opposing the electron motion, and modifying the resonant frequencies. In effect, the electromagnetic waves emitted from one region on the nanoparticle propagate through space, suffer a phase delay, and then interact with another nanoparticle region.

The problem is greatly simplified when the metal particles are much smaller than the wavelength of light. Under this condition the magnetic fields from the oscillating surface charges are small. Magnetic effects scale with the wave number k and the displacement electric fields reacting back on the surface charges scale as k^2. For very small metal particles we find that the electric effects decouple from the magnetic effects and the problem takes a mathematical form identical to that in electrostatics. Another way to see this is to write down the electric field radiated from an oscillating dipole $\mathbf{p}$ in direction $\hat{r}$ (Jackson, 1975):

$$\mathbf{E} = \frac{e^{ikr}}{4\pi\epsilon_0 r^3}\{(kr)^2(\hat{r}\times\mathbf{p})\times\hat{r} - ikr[3\hat{r}(\hat{r}\cdot\mathbf{p}) - \mathbf{p}]\} + \frac{e^{ikr}}{4\pi\epsilon_0 r^3}[3\hat{r}(\hat{r}\cdot\mathbf{p}) - \mathbf{p}]. \quad (1)$$

For distances such that $kr \ll 1$ the last term in Eq. (1) contributes the most to the electric field. This is the radiation near field, which has exactly the same form as the electrostatic result: that is, "the fields in the near zone are dominantly electric in nature" (Jackson, 1975). This near field dominates the interaction between closely spaced metal structures, which leads us to consider an approximate description of LSPs and their interactions based on an electrostatic method.

A. The electrostatic eigenvalue problem

The electrostatic theory describing the LSPs in nanoparticles with dimensions much smaller than the wavelength of light has its origin in potential theory, which describes systems of charges and dipoles and the potentials they produce (Kellog, 1929). The method was used to model the energy loss of electrons to surface plasmons when passing by a metal particle (Ouyang and Isaacson, 1989). As we show, the solution is found from an eigenvalue problem describing the self-consistent charge distributions or standing waves on the surface of a metal particle. The eigenvalues determine the resonances and the method can be considered a form of spectral theory. Such theories were investigated by Bergman (1978, 1979a, 1979b, 1979c, 1982), Kantor and Bergman (1982), and Bergman and Stroud (1992) who used them to model the electromagnetic properties of mixtures of metal particles and dielectrics.

The electrostatic result can be derived from an order expansion of Maxwell's equations (Mayergoyz, Fredkin, and Zhang, 2005) that identifies the relative importance of the different electromagnetic fields in the electrostatic problem. In essence, the zeroth order term is the interaction between the electric fields and the dielectrics, which results in the electrostatic formulation. The first-order term gives the magnetic field created by the oscillating charge distributions. This, in itself, does not affect the electrostatic result and means that we can use the electrostatic equations to predict the magnetic fields associated with LSPs, with effects such as enhanced chirality of electromagnetic fields (Davis and Hendry, 2013). The second-order term represents the electric induction created by the time-varying first-order magnetic field, which interacts back on the surface charges. It is the neglect of this and higher terms that limits the electrostatic method. These higher-order terms are small when the dimension d of the plasmonic system obeys $\epsilon_b(kd)^2 \ll 1$, where ϵ_b is the permittivity of the background medium.

The origin of the surface plasmon mode is a self-sustained surface charge oscillation: an electric charge on the surface of the metal produces an electric field that interacts with other charges on the metal surface [Figs. 1(a) and 1(b)]. The electric field from a charge at some point $\mathbf{r}'$ extends through the background medium of electric permittivity ϵ_b surrounding the metal and then penetrates the metal surface at another point $\mathbf{r}$ inducing a surface charge σ. The amount of surface charge induced at $\mathbf{r}$ is found from the discontinuity of the electric field through the metal surface $(\mathbf{E}_b - \mathbf{E}_m)\cdot\hat{n} = \sigma/\epsilon_0$ that depends on the direction of the surface normal $\hat{n}$. It is straightforward to show that a surface charge distribution σ produces an electric field $\mathbf{E}_b\cdot\hat{n} = \sigma/2\epsilon_0$ on the space outside it and $\mathbf{E}_m\cdot\hat{n} = -\sigma/2\epsilon_0$ on the inside of the surface.

However, all charges on the metal surface contribute to this surface charge, and likewise this charge produces an electric field that also interacts with all points on the metal surface. The problem is to find the distribution of surface charges in a self-consistent manner. We first write Coulomb's law for the electric field from the electric charge $q(\mathbf{r}') = \sigma(\mathbf{r}')dS'$ arising from each patch of surface with area dS':

$$\mathbf{E}(\mathbf{r}) = \frac{1}{4\pi\epsilon_0}\oint \sigma(\mathbf{r}')\frac{(\mathbf{r}-\mathbf{r}')}{|\mathbf{r}-\mathbf{r}'|^3}dS', \quad (2)$$

where, in principle, $\mathbf{r}$ can be any point in space. However, when $\mathbf{r}$ locates a point on the surface, the total electric field arises from Eq. (2) plus the charge at $\mathbf{r}$ given by the boundary condition on the normal component (Kellog, 1929). Thus the normal components of the fields at the surface in the metal and the dielectric are given by

$$\mathbf{E}_{m,b}(\mathbf{r})\cdot\hat{n} = \mp\frac{\sigma(\mathbf{r})}{2\epsilon_0} + \frac{1}{4\pi\epsilon_0}\oint \sigma(\mathbf{r}')\frac{\hat{n}\cdot(\mathbf{r}-\mathbf{r}')}{|\mathbf{r}-\mathbf{r}'|^3}dS'. \quad (3)$$

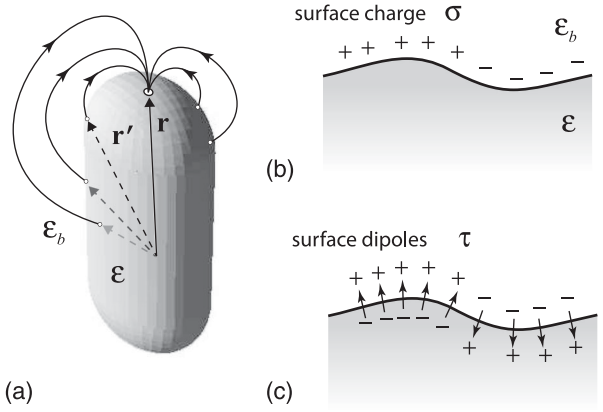

FIG. 1. The surface charges and surface dipoles that give rise to localized surface plasmon resonances. (a) The charge at each point $\mathbf{r}$ induced by the electric fields from all the other charges at $\mathbf{r}'$ distributed over the surface of a nanoparticle, (b) the LSP can be described by a distribution of surface charges σ, (c) or by a double layer of charge that is modeled by a distribution of surface dipoles τ.

Since the normal component of the electric displacement vector $\mathbf{D} = \epsilon\mathbf{E}$ is continuous across a boundary, we can relate the fields at either side of the metal surface $\epsilon_m \mathbf{E}_m \cdot \hat{n} = \epsilon_b \mathbf{E}_b \cdot \hat{n}$. Placing the electric fields from Eq. (3) into this boundary condition leads to the following condition required for self-consistency (Ouyang and Isaacson, 1989; Mayergoyz, Fredkin, and Zhang, 2005):

$$\sigma(\mathbf{r}) = \frac{\gamma}{2\pi} \oint \sigma(\mathbf{r}') \frac{\hat{n} \cdot (\mathbf{r} - \mathbf{r}')}{|\mathbf{r} - \mathbf{r}'|^3} dS', \tag{4}$$

where the electric permittivities of the metal $\epsilon_m(\omega)$ and of the surrounding, or background, medium ϵ_b are related to the eigenvalue γ by

$$\gamma[\epsilon_m(\omega) + \epsilon_b] = \epsilon_m(\omega) - \epsilon_b. \tag{5}$$

The equation for the induced surface charge has the form of an integral eigenvalue problem $(L - \lambda_L)\sigma = 0$, where L is the integral operator, $\lambda_L = 2\pi/\gamma$ is its eigenvalue, and σ is the eigenfunction. For simplicity we refer to γ as the eigenvalue of the solution, although strictly speaking the eigenvalue problem yields λ_L. The eigenvalue is found by solving the eigenvalue problem (4) where the solution gives real functions $\sigma(\mathbf{r})$ and real eigenvalues $\gamma \geq 1$ (Mayergoyz, Fredkin, and Zhang, 2005). Given the background permittivity ϵ_b one can then use Eq. (5) to deduce the permittivity ϵ_m required to fulfill self-consistency. For metals, the electric permittivity at optical frequencies is complex, since the imaginary part characterizes losses, in which case Eq. (5) can determine only the real part $\mathrm{Re}\epsilon_m$. Note that Eq. (4) can be deduced from the exact solution of Maxwell's equations in the low frequency limit (Mäkitalo, Kauranen, and Suuriniemi, 2014). As mentioned, the equation also results from a series expansion of the electromagnetic fields where the backreaction of the magnetic field on the induced surface charges is neglected, which is valid when $\epsilon_d(kd)^2 \ll 1$ with d the characteristic dimension of the structure (Mayergoyz, Fredkin, and Zhang, 2005). This condition results in the last term in Eq. (1) dominating, which is the electrostatic or near-field term.

Once the eigenvalue γ has been found and a background medium specified, Eq. (5) requires the electric permittivity ϵ to satisfy $\epsilon(\omega) = \epsilon_b(1+\gamma)/(1-\gamma)$. With usual dielectrics $\epsilon_b > 0$, and given that $\gamma \geq 1$, then Eq. (5) is satisfied only for materials with $\epsilon(\omega) < 0$. This is mainly the case for metals, semimetals, and some semiconductors. The electrostatic problem (4) is real and gives only the real part of the metal permittivity. Furthermore, the electric permittivity of a metal is negative and changes with frequency. The frequency ω_R at which the real part of the metal permittivity satisfies the eigenvalue condition is the frequency at which the surface charges oscillate: this is, in fact, the LSP resonance. Since these resonances arise as a consequence of an electrostatic or near-field condition, these are sometimes referred to as electrostatic resonances. Figure 2 shows the real and imaginary parts of the relative electric permittivities of gold and silver (Weaver and Frederikse, 2006) and the wavelengths at which the fundamental dipole resonance of the example nanoparticle will resonate in air, based on the real part of the permittivity. Because the electrostatic method neglects the action of the magnetic field on the induced surface charge, the estimate of the resonance frequency of the fundamental mode is accurate to around 10% and blueshifted relative to the actual frequency. The estimate becomes worse as the dimension d of the structure increases such that the condition $\epsilon_b(kd)^2 \ll 1$ is no longer satisfied (Davis, Vernon, and Gómez, 2009b). Interestingly, the estimates of the resonances of higher-order modes lose accuracy more slowly, suggesting that d should really characterize the size of the half wavelengths of the modes (Davis, Vernon, and Gómez, 2009b).

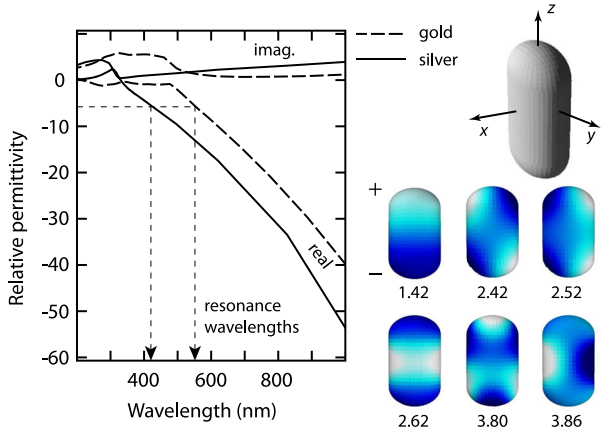

FIG. 2. The first six eigenmodes of an example particle, which is a flattened cylinder with rounded ends with dimensions in the ratio $L_z : D_y : D_x = 2.6 : 1.5 : 1.0$. The gray level (color) represents the surface dipole distribution and the numbers are the eigenvalues. Also shown are the real and imaginary parts of the relative electric permittivities of gold and silver. For the fundamental dipole mode $\gamma_1^1 = 1.42$ placed in air $\epsilon_b = 1$ the resonance occurs where the metal permittivity $\mathrm{Re}\epsilon = \epsilon_b(1+\gamma)/(1-\gamma) = -5.76$ at wavelengths 554 nm for gold and 426 nm for silver as shown.

As with all eigenvalue problems we obtain a series of eigenvalues and an associated set of eigenfunctions. We label these to distinguish them from one another. We associate the kth eigenfunction $\sigma_n^k(\mathbf{r})$ with the kth eigenvalue γ_n^k of particle n. Examples of the eigenfunctions of a "flattened cylinder" are shown in Fig. 2 which were found by numerically solving Eq. (4) using the method of Mayergoyz, Fredkin, and Zhang (2005) [see also the freely available boundary element method Matlab toolbox by Hohenester and Trugler (2012) in its electrostatic limit]. Analytical solutions are also possible for special nanoparticle geometries such as a sphere, for which we show in Appendix A the eigenmodes and eigenvalues obtained by solving Eq. (4).

The eigenfunctions of Eq. (4) are the standing waves on the surface of the particle, not unlike the standing waves one might find on the surface of a vibrating membrane. These surface charge distributions have a complicated multipolar nature, meaning the distributions can be expanded in terms of dipoles, quadrupoles, hexapoles, and so on (Wei *et al.*, 2010). Since electric charges accumulate at boundaries, the fundamental mode of any structure has a half wavelength standing wave with positive charge on one boundary and negative charge on the opposite boundary. This charge distribution has a strong dipole moment, such as the first mode shown in

Fig. 2. This is common to most nanostructures and we exploit this property in Sec. III. Each standing wave is associated with an eigenvalue which is a real valued number greater than 1 (Mayergoyz, Fredkin, and Zhang, 2005). Strictly speaking, the surface charges oscillate in time so we should multiply the eigenfunctions by $e^{-i\omega t}$.

The problem as outlined in Eq. (4) is scale independent. Changing the dimensions of length such as $r \to \beta r$ leaves the equation unchanged since all powers of β cancel. Thus we find that the eigenfunctions depend only on the geometry of the nanoparticle, and, in particular, on its aspect ratio, but not on its actual size. This is a consequence of the electrostatic or near-field approximation used in this theory. Another important feature of Eq. (4) is that it places no restrictions on the continuity of the surface—that is the surface may consist of several pieces. In this respect the eigenvalue problem can be applied to two or more particles of arbitrary shape and it will give the LSP resonances of the combination (Gómez, Vernon, and Davis, 2010). We use this fact in Sec. II.E to derive an expression describing the interaction between LSPs on multiple particles.

Surface charges are one way to describe an electrostatic problem but we can also use surface dipole distributions. In this model the boundary condition comes from a change in the *electric potential* across the surface, which is then related to the surface dipole moment $\phi_b - \phi_m = \tau/\epsilon_0$ (Jackson, 1975). In effect, an electric charge on the surface has a companion opposite charge just below the surface, creating a surface dipole moment $\tau\hat{n}$, also known as a double layer (Kellog, 1929), aligned parallel to the surface normal $\hat{n}$ [Fig. 1(c)]. It is straightforward to determine the electric potentials across the double layer resulting in expressions similar to Eq. (3). Then we find that the surface dipole moment also obeys an eigenvalue problem (Mayergoyz, Fredkin, and Zhang, 2005)

$$\tau(\mathbf{r}) = \frac{\gamma}{2\pi} \oint \tau(\mathbf{r}') \frac{\hat{n}' \cdot (\mathbf{r}' - \mathbf{r})}{|\mathbf{r}' - \mathbf{r}|^3} dS'. \tag{6}$$

This is the "dual" problem associated with the surface charge eigenvalue equation.

Both Eqs. (4) and (6) are equivalent and lead to the same eigenvalue. The usefulness of Eq. (6) lies in the property that the surface charge and surface dipole eigenfunctions form a biorthogonal set $\oint \tau_m^j(\mathbf{r})\sigma_n^k(\mathbf{r})dS = \delta_{mn}\delta^{jk}$ (Mayergoyz, Fredkin, and Zhang, 2005). The integral is zero unless the eigenfunctions are associated with the same particle and the same eigenvalue. We use superscripts on the delta function to remind us these refer to the eigenmodes (not to be confused with the notation used in relativity to refer to covariant and contravariant vectors). This is similar to the orthonormal set of functions ψ_n used in quantum mechanics as derived from the Schrödinger equation. The difference is that the quantum wave equation is Hermitian so that its adjoint is equal to the complex conjugate resulting in complex eigenfunctions that are orthonormal $(1/V)\int \psi_n^*(\mathbf{r})\psi_m(\mathbf{r})dV = \delta_{nm}$. Here the electrostatic eigenfunctions are real and do not have this property, which requires the use of an auxiliary equation resulting in a biorthogonal pair σ_n^k and τ_m^j. In the language of linear algebra, these two functions form a left and a right eigenvector pair.

B. LSP excitation amplitudes

In the previous section we described the LSPs in terms of the natural resonant modes of a nanoparticle that has a negative electric permittivity. The natural resonances are described mathematically by surface charge eigenfunctions, surface dipole eigenfunctions, and their eigenvalues. The question arises as to which of these modes, if any, are excited when an electromagnetic wave is incident on the particle and how strong are the excitations?

This problem was addressed in the context of nanoparticle excitation by pulsed laser sources (Mayergoyz, Zhang, and Miano, 2007). The electric field $\mathbf{E}_0(\mathbf{r})\exp(-i\omega t)$ of the incident light excites an oscillating surface charge $\sigma(\mathbf{r},\omega)\exp(-i\omega t)$ that varies with position over the nanoparticle surface. This surface charge can be represented by a linear combination of the eigenmodes of the particle $\sigma(\mathbf{r},\omega) = \sum_k a_n^k(\omega)\sigma_n^k(\mathbf{r})$. The expansion coefficient $a_n^k(\omega)$ represents the strength of the excitation of the kth LSP mode: the *excitation amplitude*. By applying the boundary condition in which the normal components of the electric displacement across the metal surface are continuous, then $\epsilon_m(\omega)(\mathbf{E}_0 + \mathbf{E}_m)\cdot\hat{n} = \epsilon_b(\mathbf{E}_0 + \mathbf{E}_b)\cdot\hat{n}$. Across the boundary at a position $\mathbf{r}$, the normal component of the electric field has a discontinuity given in Eq. (3). Substituting for $\mathbf{E}_m$ and $\mathbf{E}_b$, expanding the surface charge in terms of eigenfunctions, multiplying by $\tau_m^j(\mathbf{r})$, integrating over the surface, and using the biorthogonality condition, leads to an equation for the excitation amplitude

$$\begin{aligned} a_m^j(\omega) &= f_m^j(\omega) \oint \tau_m^j(\mathbf{r}')\hat{n}'\cdot\mathbf{E}_0(\mathbf{r}')dS' \\ &\approx f_m^j(\omega)\mathbf{p}_m^j\cdot\mathbf{E}_0, \end{aligned} \tag{7}$$

where

$$f_m^j(\omega) = \frac{2\gamma_m^j\epsilon_b[\epsilon_m(\omega) - \epsilon_b]}{\epsilon_b(\gamma_m^j + 1) + \epsilon_m(\omega)(\gamma_m^j - 1)}. \tag{8}$$

We introduced a factor $f_m^j(\omega)$, which is the polarizability per unit volume. As we show this factor plays a key role in determining the LSP resonance and includes information on the amplitudes and the phases.

At the subwavelength scale where the electrostatic limit applies, the incident electric field is approximately constant over the nanoparticle surface. Under this condition $\mathbf{E}_0$ can be taken out of the integral leading to $a_m^j(\omega) \approx f_m^j(\omega)\mathbf{p}_m^j\cdot\mathbf{E}_0$ as given in Eq. (7), where $\mathbf{p}_m^j = \oint \tau_m^j(\mathbf{r}')\hat{n}'dS'$ represents the average dipole moment associated with the eigenfunction τ_m^k. This dipole moment is proportional to the actual dipole moment of the LSP mode k in the nanoparticle, differing only by a scale factor. Indeed, the true dipole moment is just $\mathbf{p}_m(\omega) = \sum_k a_m^k(\omega)\mathbf{p}_m^k$. In what follows we refer to $\mathbf{p}_m^k$ as the *eigenfunction dipole moment* to distinguish it from the true dipole moment $\mathbf{p}_m$. Note that we can also write the

eigenfunction dipole moment in terms of the surface charge $\mathbf{p}_m^j = \oint \sigma_m^j(\mathbf{r}')\mathbf{r}' dS'$ which is identical to the eigenfunction dipole moment derived from τ_n^k if the eigenfunctions are properly normalized (Davis, Gómez, and Vernon, 2010b).

The excitation amplitude $a_m^j(\omega)$ represents the strength of the LSP mode j excited on nanoparticle m by the incident light field at frequency ω. The frequency dependence is contained within the factor $f_m^j(\omega)$. This factor becomes very large when the real part of the denominator is zero, $\mathrm{Re}[\epsilon_b(\gamma_m^j + 1) + \epsilon(\omega)(\gamma_m^j - 1)] = 0$, which is the same relationship of Eq. (5) we found previously linking the eigenvalue to the electric permittivities of the nanoparticle and the surrounding medium. As an example, the eigenvalue for the fundamental resonance of a sphere is $\gamma = 3$ (see Appendix A). When placed in Eq. (8) the resonance factor is $f_s^1 = 3\epsilon_b(\epsilon_m - \epsilon_b)/(\epsilon_m + 2\epsilon_b)$ which we identify as the optical polarizability of a small metal particle (Bohren and Huffman, 1983) with the Frölich resonance condition $\epsilon_m + 2\epsilon_b = 0$. The excitation amplitude is a complex quantity because it contains, through f_m^j, information about the phase of the LSP oscillation relative to the phase of the driving field $\mathbf{E}_0$, which in turn is complex because the metal permittivity $\epsilon(\omega)$ is complex. For frequencies away from resonance we expect f_m^j to become small, reducing the strength of the LSP.

The complex dependence of $f_m^j(\omega)$ can be made explicit using an approximate expression for the metal permittivity based on a Drude model (Kittel, 1956; Ashcroft and Mermin, 1976). In this model the electric permittivity has the form $\epsilon_m(\omega) \approx 1 - \omega_P^2/\omega(\omega + i\Gamma)$, where ω_P is the bulk plasma frequency of the metal and Γ is a loss term. Using this expression in Eq. (8), expanding the result about the resonance frequency ω_R and assuming the loss Γ is small, then the frequency-dependent factor can be approximated by

$$f_m^j(\omega) \approx -\left(\frac{2\gamma_m^j \epsilon_b^2 {\omega_m^j}^3}{(\gamma_m^j - 1)^2\omega_P^2}\right)\frac{1}{(\omega - \omega_m^j + i\Gamma_m^j/2)} = \frac{-A_m^j}{\omega - \omega_m^j + i\Gamma_m^j/2}, \tag{9}$$

where ω_m^j is the resonance frequency of mode j of particle k, Γ_m^j is the full width at half maximum (FWHM) of the resonance, and A_m^j is a positive scale factor that depends on the resonant mode and the permittivity of the background medium (Appendix B has a detailed derivation of this approximate form).

Equation (9) is important because it shows how the LSP resonance changes with frequency and it enables us to model in a simple way the phase variations of the resonance relative to the incident electric field. The equation is approximate and is valid only close to the LSP resonance. This equation, along with Eq. (7), is the key algebraic expression that we use to model LSP resonances in single metal nanoparticles. As we show later, the properties of LSPs in ensembles of metal nanoparticles can be obtained from the mathematical form of Eqs. (7) and (9) without needing to know the actual values of the resonance frequency, the FWHM, the scale factor, or even the eigenvalues or eigenfunctions. This is analogous to problems in quantum mechanics (based on Dirac's bra-ket notation $\langle\psi|$ and $|\psi\rangle$) in which many properties of quantum systems can be determined using the linear algebra of the operators, the wave functions, and their orthogonality properties without requiring actual details of the spatial dependence or their functional form (Cohen-Tannoudji, Diu, and Laloe, 1977).

C. Optical theorem, energy conservation, and radiation

The optical theorem is an expression of energy conservation. It equates the electromagnetic energy scattered from a particle in the forward direction to the energy absorbed by it (Jackson, 1975). It is instructive to demonstrate how the approximations in the electrostatic method cause it to fail, which provides insight into the radiation mechanism and why the resonances lead to energy storage. In what follows we use expressions given by Jackson (1975) converted to SI units. We assume an electromagnetic plane wave in vacuum with an electric field $\mathbf{E}(\mathbf{r}, t) = \mathbf{E}_0 \exp(i\mathbf{k}\cdot\mathbf{r} - i\omega t)$ and magnetic field $\mathbf{H}(\mathbf{r}, t) = \epsilon_0 c(\hat{k} \times \mathbf{E}_0)\exp(i\mathbf{k}\cdot\mathbf{r} - i\omega t)$, where ϵ_0 is the permittivity of free space. The complex Poynting vector for time harmonic fields is $\mathbf{S} = (\mathbf{E} \times \mathbf{H}^*)/2$. The real part of $\mathbf{S}$ is the radiated energy, whereas the imaginary part represents the reactive or stored energy and its alternating flow.

1. Absorption

The rate at which work is done per unit volume for time-averaged quantities is given by the real part of $\dot{u} = \mathrm{Re}(\mathbf{J}^* \cdot \mathbf{E})/2$ in terms of the induced current density $\mathbf{J}\exp(-i\omega t)$ and the electric field that drives it. The current density at position $\mathbf{r}'$ on the surface of plasmonic structure m is given by the time rate of change of the total dipole moment $\partial \mathbf{p}_m(\mathbf{r}', t)/\partial t = -i\omega \sum_k a_m^k \tau_m^k(\mathbf{r}')\hat{n}' \exp(-i\omega t)$, where $\mathbf{p}_m(\mathbf{r}', t) = \sum_k a_m^k \tau_m^k(\mathbf{r}')\hat{n}' \exp(-i\omega t)$ is written as a sum over the modes k. The power absorbed per unit volume is then

$$\dot{u}_m = -(\omega/2)\mathrm{Im}\sum_k a_m^{k*} \oint \tau_m^k(\mathbf{r}')\hat{n}' \cdot \mathbf{E}(\mathbf{r}')dS', \tag{10}$$

which is integrated over the particle surface. We take the imaginary part since $\mathrm{Re}(iZ) = -\mathrm{Im}(Z)$ for any complex function Z. As before we assume that $\mathbf{E}(\mathbf{r}') \approx \mathbf{E}_0$ is approximately constant over the surface and replace the integral with the eigenvalue dipole moment. Furthermore we have $a_m^k \approx f_m^k \mathbf{p}_m^k \cdot \mathbf{E}_0$ so that

$$\dot{u}_m \approx -(\omega/2)\sum_k \mathrm{Im} f_m^{k*} |\mathbf{p}_m^k \cdot \mathbf{E}_0|^2. \tag{11}$$

The Poynting vector gives us the incident intensity $I = \epsilon_0 c|E_0|^2/2$ in terms of the electric field $\mathbf{E}_0$. For a single resonance mode with a dipole moment aligned to the incident field, the absorption cross section C_{abs} is the ratio of the absorbed power per unit volume per incident intensity

$$C_{\mathrm{abs}} = \dot{u}_m/I = k(p_m^k)^2 \mathrm{Im}\left(\frac{2\gamma(\epsilon_0 - \epsilon_m^*)}{\epsilon_0(\gamma + 1) + \epsilon_m^*(\gamma - 1)}\right). \tag{12}$$

For a sphere of radius R it has been shown that $(p_m^k)^2 = 4\pi R^3/3$ is equal to the volume (Davis, Gómez, and Vernon, 2010b) and that $\gamma = 3$. Then

$$C_{\text{abs}} = k4\pi R^3 \text{Im}\left(\frac{\epsilon_0 - \epsilon_m^*}{2\epsilon_0 + \epsilon_m^*}\right), \tag{13}$$

which is the usual expression for the absorption cross section of a small sphere (Bohren and Huffman, 1983). Note that Eq. (12) represents the absorption of the fundamental LSP mode for particles of any shape, characterized by γ. In the theory of light scattering from particles, nonspherical shapes are usually approximated by ellipsoids for which the absorption cross section is given in terms of a shape factor L, commonly referred to as the depolarization factor. Comparing Eq. (12) to the expression for scattering from an ellipsoid, we can relate the depolarization factor to the eigenvalue γ, with the result $L = (\gamma - 1)/2\gamma$ (Vernon *et al.*, 2010). Equation (12) is more general since there is no assumption about the shape other than it is much smaller than the wavelength of light.

2. Radiation

The power radiated from the LSP is obtained from the real part of the Poynting vector. In the electrostatic approximation, the electric field is given by Eq. (2) with the surface charge on nanostructure m expanded in surface charge eigenfunctions $\sigma_m(\mathbf{r}') = \sum_k a_m^k \sigma_m^k(\mathbf{r}')$. The magnetic field is obtained from the Biot-Savart law that involves the current density in the metal arising from the oscillating dipole moment $-i\omega\sum_k a_m^k \tau_m^k(\mathbf{r}')\hat{n}'$ as before,

$$\mathbf{H}(\mathbf{r}) = \frac{-i\omega}{4\pi}\sum_k a_m^k \oint \tau_m^k(\mathbf{r}')\frac{\hat{n}' \times (\mathbf{r} - \mathbf{r}')}{|\mathbf{r} - \mathbf{r}'|^3} dS'. \tag{14}$$

For simplicity we consider a single dominant mode and keep only one term in the sum over the eigenfunctions. Then the Poynting vector is

$$\mathbf{S} = \frac{i\omega}{16\pi^2}|a_m^k|^2 \mathbf{s}(\mathbf{r}), \tag{15}$$

with

$$\mathbf{s}(\mathbf{r}) = \oint\oint \sigma_m^k(\mathbf{r}')\tau_m^k(\mathbf{r}'')\frac{(\mathbf{r} - \mathbf{r}') \times \hat{n}'' \times (\mathbf{r} - \mathbf{r}'')}{|\mathbf{r} - \mathbf{r}'|^3 |\mathbf{r} - \mathbf{r}''|^3} dS' dS''. \tag{16}$$

Since $\mathbf{s}(\mathbf{r})$ and $|a_m^k|^2$ are real, the Poynting vector is purely imaginary and the radiated power, given by the real part of $\mathbf{S}$, is zero. Thus in the electrostatic theory there is no radiation. The purely imaginary Poynting vector represents the stored energy associated with the plasmon, which is not surprising since we neglected the induction of an electric field by the magnetic field. The magnetic field oscillates 90° out of phase with the electric field and therefore can never generate a wave propagating in free space. Including second- and higher-order terms leads to a phase shift in the magnetic field with a small in-phase component (Mayergoyz, Fredkin, and Zhang, 2005). It is this component that is responsible for radiation. Thus to first order in the fields, the plasmon captures the optical energy and loses it only by absorption. The optical theorem is not obeyed. Since the electrostatic method does not include the electromotive force of the magnetic field, the method is unable to predict the properties of structures that exploit magnetic induction, such as split-ring resonators (Lezec, Dionne, and Atwater, 2007).

Light radiated from these structures can be included as a separate effect. Since dipole radiation dominates over higher-order multipoles, we can write the radiated power in terms of the LSP dipole moments $\mathbf{p}_m = \sum_k a_m^k(\omega)\mathbf{p}_m^k$. The time-averaged power per solid angle radiated in the far field direction $\hat{n}$ can be written in the form (Jackson, 1975)

$$\frac{dP}{d\Omega} = \frac{ck^4}{32\pi^2\epsilon_b}(\hat{n} \times \mathbf{p}) \cdot (\hat{n} \times \mathbf{p}^*), \tag{17}$$

where c is the speed of light, ϵ_b is the relative permittivity of the dielectric occupying the space, and $\mathbf{p}^*$ is the complex conjugate of the dipole moment.

For a particle with a single LSP mode it is clear that the radiated power is proportional to $|a_m|^2$. The scattering cross section of a particle $C_{\text{sca}} = (k^4/6\pi)|\mathbf{p}/E_0|^2$ is also proportional to the modulus square of the dipole moment (Bohren and Huffman, 1983) leading to a similar dependence on $|a_m|^2$ of the excitation amplitude. This provides a convenient way to estimate the relative strength of the light reradiated by the LSPs.

3. Radiation damping

The electromagnetic energy radiated by an oscillating surface charge density (with an associated dipole moment $\mathbf{p}$) is one mechanism by which a resonance is damped, increasing the spectral linewidth, and decreasing the quality factor. The effect of the radiated electromagnetic field on the LSP can be modeled by a "self-field"(Meystre and Sargent, 1998) $\mathbf{E}_{\text{rad}} = (ik^3/6\pi\epsilon_b)\mathbf{p}$ that perturbs the oscillation ($k = \omega/c$). This field can be included in the following expression for the excitation amplitude of Eq. (7) (Davis, Vernon, and Gómez, 2009a):

$$\begin{aligned} a_m^j(\omega) &= f_m^j(\omega)\mathbf{p}_m^j \cdot \left(\mathbf{E}_0 + i\frac{k^3}{6\pi\epsilon_b}\mathbf{p}\right) \\ &= f_m^j(\omega)\mathbf{p}_m^j \cdot \left(\mathbf{E}_0 + i\frac{k^3}{6\pi\epsilon_b}\sum_n a_m^n(\omega)\mathbf{p}_m^n\right), \end{aligned} \tag{18}$$

which leads to

$$a_m^j(\omega) = \left[\delta^{jn} - i\frac{f_m^j(\omega)k^3}{6\pi\epsilon_b}\sum\nolimits_n \mathbf{p}_m^j \cdot \mathbf{p}_m^n\right]^{-1} f_m^j(\omega)\mathbf{p}_m^j \cdot \mathbf{E}_0. \tag{19}$$

As an example, Eq. (19) for a particle with a single resonant mode can be written as

$$a_m^j(\omega) \approx \frac{-A_m^j \mathbf{p}_m^j \cdot \mathbf{E}_0}{\omega - \omega_m^j + i[\Gamma_m^j/2 + A_m^j k^3 (p_m^j)^2/6\pi\epsilon_b]}, \quad (20)$$

where Eq. (9) has been used for $f_m^j(\omega)$ [cf. Carminati *et al.* (2006)]. This equation explicitly shows how the LSP resonance width, given by the imaginary part of the denominator, increases with increasing radiation (dipole moment).

The excitation amplitude of the jth resonance, as mentioned, is large for modes with a strong dipolar character. However, these modes also have associated strong radiation and therefore lead to large radiation damping (Sönnichsen *et al.*, 2002) according to the denominator of Eq. (20) which thus limit the near-field strength of the LSP (Wokaun, Gordon, and Liao, 1982).

D. Properties of isolated metal nanostructures

The electrostatic approximation described predicts some useful properties of LSP resonances.

(i) For very small nanoparticles where the incident electric field is constant over the nanoparticle surface, we observe that LSP modes with a zero dipole moment $\mathbf{p}_m^k = 0$ are not excited [Eq. (7)]. Two examples are the second and fourth modes in Fig. 2 with $\gamma_1^2 = 2.42$ and $\gamma_1^4 = 2.62$, which are predominantly quadrupolar in nature with very small dipole moments. In practice there is always a small variation of the electric field over the nanoparticle surface enabling these modes to be excited. However, the excitations are generally very weak and not usually observed unless the nanoparticles are large. Thus, we note that only LSP modes with nonzero dipole moments are usually excited (Yang *et al.*, 2010).

(ii) The phase ϕ of the LSP relative to the phase of the incident light depends on frequency according to $\tan\phi = -\Gamma_m^k/2(\omega - \omega_m^k)$ which is obtained from the ratio of the imaginary to the real parts of Eq. (9). Well below resonance the phase is approximately zero $\phi \approx 0$, it passes through 90° on resonance $\phi = \pi/2$, and approaches 180° above resonance $\phi \to \pi$. This is the characteristic behavior of a driven oscillator ubiquitous in physics. As shown in Sec. III, the coupling between LSPs leads to coupled oscillators and frequency splitting, another property that is found in many different fields of physics.

(iii) The LSP mode is not excited if the incident electric field is perpendicular to the LSP dipole moment whereby $\mathbf{p}_m^j \cdot \mathbf{E}_0 = 0$. Therefore the excitation of a given LSP mode depends on the polarization of the incident light. In addition, the electric field of the light radiated from the LSP is polarized with a direction related to the orientation of the dipole moment, as in the far field term of Eq. (1). Using a vector identity it is possible to write $(\hat{r} \times \mathbf{p}) \times \hat{r} = \mathbf{p} - (\hat{r} \cdot \mathbf{p})\hat{r}$. In a direction normal to the LSP dipole moment, the radiated field is $\mathbf{E}_{\text{rad}} \propto \mathbf{p}_m^j(\mathbf{p}_m^j \cdot \mathbf{E}_0)$ which can have a polarization different from the incident field $\mathbf{E}_0$. This is a useful property of metal nanoparticles with nondegenerate LSP modes that can be used to manipulate the polarization direction of a light wave (Ming *et al.*, 2009; Kosako, Kadoya, and Hofmann, 2010).

It is worth noting that symmetric nanoparticles, such as cylinders and spheres, have multiple degenerate LSP modes with orthogonal dipole moments. A cylinder has two orthogonal modes across its diameter whereas a sphere has three (details on this last example are given in Appendix A). For such structures we must include all the degenerate modes in the interaction, so that the radiated field is $\mathbf{E}_{\text{rad}} \propto \sum_j \mathbf{p}_m^j(\mathbf{p}_m^j \cdot \mathbf{E}_0)$. For example, a sphere with all three LSP dipole moments $\mathbf{p}_m^j = \mathbf{p}_m^1 \hat{x}^j$ having identical magnitudes but different orientations given by the orthogonal unit vectors $\hat{x}^j$, the field radiated by the LSPs $\mathbf{E}_{\text{rad}} \propto (p_m^1)^2 \sum_{j=1}^3 \hat{x}^j(\hat{x}^j \cdot \mathbf{E}_0) = (p_m^1)^2 \mathbf{E}_0$ has a polarization parallel to the incident field, so that no polarization conversion arises.

1. An example with multiple LSP resonances

Structures that have multiple LSP modes with nonzero dipole moments can show interesting optical properties that depend on the polarization of the incident light. As an example, we apply the algebraic model to a single metal structure that has multiple degenerate or near degenerate modes and show how the structure behaves with circularly polarized light (Eftekhari and Davis, 2012). Consider the "Y"-shaped structure in Fig. 3 that has two strong dipole modes with resonances that differ in frequency by $\Delta\omega_{12}$ and dipole moments rotated from one another by θ_{12}. The circularly polarized light $\mathbf{E} = E_0(\hat{x} \pm i\hat{y})$ is incident normal

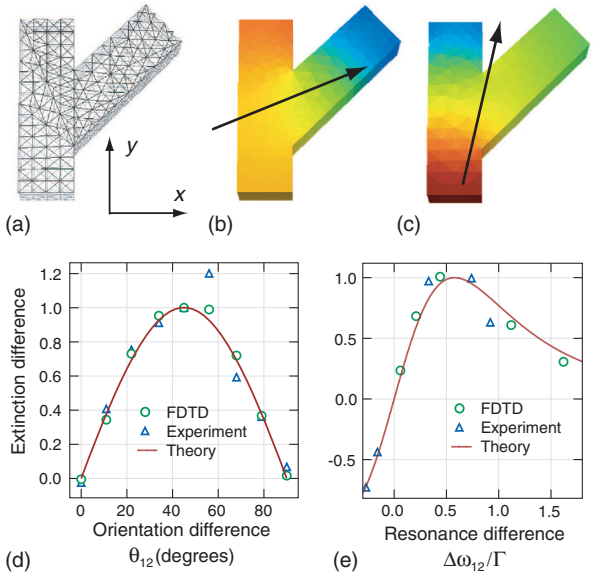

FIG. 3. An example of nonorthogonal LSP modes interacting with the handedness of circularly polarized light. (a) The numerical grid of 1296 triangles used to simulate the LSP modes (b) and (c). The structure is 3 units thick, each section is 3.5 units wide and 11.5 units long. The side section extends at 45°, (b) the fundamental dipole mode of the structure in (a) with $\gamma = 1.12$ and a dipole moment shown by the arrow, (c) the second dipole mode $\gamma = 1.21$, (d) a comparison of the theory prediction $\sin 2\theta$ for the extinction difference between left and right circularly polarized light as a function of angle θ_{12} compared with experimental data on a set of plasmonic systems with two nonorthogonal modes and with a finite-difference time-domain (FDTD) simulation, and (e) as per (d) but as a function of the resonance difference between the two modes. Adapted from Eftekhari and Davis, 2012.

to the surface in the x-y plane. The $\pm$ sign determines the handedness of the polarization. The radiated power Eq. (17) scattered normal to the plane depends on $(\hat{n}\times\mathbf{p}_m)\cdot(\hat{n}\times\mathbf{p}_m^*)=\mathbf{p}_m\cdot\mathbf{p}_m^*$ since the polarization is perpendicular to $\hat{n}$. Assuming only two dominant modes with $\mathbf{p}_m=\sum_k a_m^k\mathbf{p}_m^k$ and $\mathbf{p}_m^k=p_m^k(\cos\theta_m^k\hat{x}+\sin\theta_m^k\hat{y})$ then

$$\mathbf{p}_m\cdot\mathbf{p}_m^* = |a_m^1|^2 {p_m^1}^2 + |a_m^2|^2 {p_m^2}^2 + 2\mathrm{Re}[a_m^1 a_m^{2*}]p_m^1 p_m^2\cos\theta_{12}. \tag{21}$$

We can write $a_m^1=f_m^1\mathbf{p}_m^1\cdot\mathbf{E}=|f_m^1|p_m^1E_0\exp(i\phi_m^1\pm i\theta_m^1)$, where $f_m^1=|f_m^1|\exp(i\phi_m^1)$ is a magnitude and a phase and likewise for a_m^2. Then from Eq. (21) we have

$$\begin{aligned}\mathbf{p}_m\cdot\mathbf{p}_m^* = {}& |f_m^1|^2{p_m^1}^4E_0^2+|a_m^2|^2{p_m^2}^4E_0^2\\ & +2|f_m^1||f_m^2|(p_m^1p_m^2)^2E_0^2\cos^2\theta_{12}\cos\phi_{12}\\ & \mp|f_m^1||f_m^2|(p_m^1p_m^2)^2E_0^2\sin 2\theta_{12}\sin\phi_{12},\end{aligned} \tag{22}$$

where $\phi_{12}=\phi_m^1-\phi_m^2$ is the difference in the phases of the LSP oscillations.

The key factor is the product $\sin 2\theta_{12}\sin\phi_{12}$ on the last line of Eq. (22). The scattered power, proportional to $\mathbf{p}_m\cdot\mathbf{p}_m^*$, will be sensitive to the handedness $\mp$ of the circular polarization if the dipole moments of the two resonances are neither parallel nor perpendicular, so that $\sin 2\theta_{12}\neq 0$ and optimally when $\theta_{12}=45°$. In addition there must be a phase difference between the two resonances $\phi_{12}\neq 0$ which means the two modes cannot be degenerate (must have different resonance frequencies). If both conditions are satisfied the last term in Eq. (22) is not zero. If we repeat the derivation but use the approximation for f_m^k in Eq. (9) in terms of resonance frequencies, we can show that the difference in the extinction between left and right circularly polarized light varies with the resonance difference $\omega_m^1-\omega_m^2=\Delta\omega_{12}$ according to $x/(x^2+1)^2$ with $x=\Delta\omega_{12}/\Gamma$. This has a maximum at $x=1/\sqrt{3}$ or $|\Delta\omega_{12}|=\Gamma/\sqrt{3}$ (Eftekhari and Davis, 2012).

Figures 3(d) and 3(e) show the results of experiments (Eftekhari and Davis, 2012) on a set of two-mode LSP systems and compares them with data from a FDTD numerical simulation and the results of the model. The model shows remarkable agreement with both simulations and experiment. This example demonstrates the value of a simple algebraic model in that we can deduce two nonobvious conditions relating circularly polarized light and its interaction to the properties of a metal structure exhibiting two LSP modes. The model works well because it provides a good representation of the LSP line shape and phase close to the resonance and it includes the vector interaction of the polarization of the incident light with the dipole moments of the LSP modes.

E. Coupled LSPs

One useful property of LSPs is that they enable the manipulation of the phase and polarization of optical fields (Liu *et al.*, 2005; Ebbesen, Genet, and Bozhevolnyi, 2008; Dregely *et al.*, 2011; Langguth *et al.*, 2015). This can be achieved by placing two or more metal nanoparticles in close proximity such that the evanescent electric fields from the LSPs induce electric charges, and hence new LSPs, on neighboring particles (Halas *et al.*, 2011; Gallinet *et al.*, 2013; Langguth *et al.*, 2015). Traditionally, these coupling problems are difficult to solve and are usually analyzed numerically (Brandl, Mirin, and Nordlander, 2006). However, we show that the electrostatic eigenmode method leads to very simple expressions for many of the nanoparticle configurations of interest.

In the theory previously outlined, the strength of a particular LSP resonance in an isolated nanoparticle is determined by the excitation amplitude a_m^k. If there are multiple nanoparticles, then the excitation amplitudes change. The electric field at the position of nanoparticle m arises from two sources: the incident field $\mathbf{E}_0$ and the electric fields from the LSPs on all the other nanoparticles $\sum_n\mathbf{E}_n$. These extra fields must be included in Eq. (7) for the excitation amplitude yielding a new amplitude $\tilde{a}_m^k(\omega)$ given by

$$\tilde{a}_m^k(\omega)=f_m^k(\omega)\oint\tau_m^k(\mathbf{r}_m)\hat{n}_m\cdot\left(\mathbf{E}_0+\sum_n\mathbf{E}_n(\mathbf{r}_m)\right)dS_m, \tag{23}$$

where the integral is over nanoparticle m. The electric field $\mathbf{E}_n(\mathbf{r}_m)$ at particle m arising from particle n can be found from Coulomb's law. The total surface charge associated with particle n is $\sigma_n=\sum_j\tilde{a}_n^j\sigma_n^j$ so that

$$\mathbf{E}_n(\mathbf{r}_m)=\frac{1}{4\pi\epsilon_b}\sum_j\tilde{a}_n^j(\omega)\oint\sigma_n^j(\mathbf{r}_n)\frac{\hat{n}_m.(\mathbf{r}_m-\mathbf{r}_n)}{|\mathbf{r}_m-\mathbf{r}_n|^3}dS_n. \tag{24}$$

Combining Eq. (24) with Eq. (23) and noting that the first term in Eq. (23) is just the excitation amplitude a_m^k of nanoparticle m when it is isolated, we have

$$\tilde{a}_m^k(\omega)=a_m^k(\omega)+f_m^k(\omega)\sum_{n,j}\tilde{a}_n^jG_{mn}^{kj}, \tag{25}$$

where

$$G_{mn}^{kj}=\frac{1}{4\pi\epsilon_b}\oint\oint\tau_m^k(\mathbf{r}_m)\frac{\hat{n}_m.(\mathbf{r}_m-\mathbf{r}_n)}{|\mathbf{r}_m-\mathbf{r}_n|^3}\sigma_n^j(\mathbf{r}_n)dS_ndS_m \tag{26}$$

is the Coulomb coupling from nanoparticle n to nanoparticle m. We define this coupling such that $G_{mm}^{kj}=0$. Equation (25) can be rearranged

$$\sum_{n,j}[\delta_{mn}\delta^{kj}-f_m^k(\omega)G_{mn}^{kj}]\tilde{a}_n^j(\omega)=a_m^k(\omega) \tag{27}$$

as a matrix equation, which can be written in terms of an inverse

$$\tilde{a}_n^j(\omega)=\sum_{m,k}[\delta_{mn}\delta^{kj}-f_n^j(\omega)G_{nm}^{jk}]^{-1}a_m^k(\omega). \tag{28}$$

This equation is extremely useful for describing the interaction between metal nanoparticles supporting LSP resonances. It relates the excitation $\tilde{a}_n^j(\omega)$ of the nanoparticle when it

is a member of an ensemble to the excitations $a_m^k(\omega)$ of each of the isolated nanoparticles. We know the functional form of the single particle excitations—they are given by Eqs. (7) and (9). By inverting the matrix in Eq. (28) we can determine what the excitations look like when the particles are coupled together.

The geometric coupling coefficient G_{nm}^{jk} represents the interaction of the evanescent electric fields of the LSPs. Unless we need to calculate exact numerical values, it is not usually necessary to determine its magnitude in order to understand how metal nanoparticles behave when coupled together. However, it is useful to know whether or not this factor is positive, negative, or zero. A simplified expression is obtained by imagining two particles n and m separated by a distance $\mathbf{d}_{nm}$ sufficiently large that the integrals over the nanoparticle surfaces in Eq. (26) leave $\mathbf{r}_n - \mathbf{r}_m$ almost constant. We can write $\mathbf{r}_n - \mathbf{r}_m = \mathbf{s}_n - \mathbf{s}_m + \mathbf{d}_{nm}$, where $\mathbf{s}_n$ is a small vector pointing from the center of nanoparticle n to a point on its surface, and likewise for $\mathbf{s}_m$. Then the factor $|\mathbf{r}_n - \mathbf{r}_m|^{-3} \approx d_{nm}^{-3}[1 - 3(\mathbf{s}_n - \mathbf{s}_m)\cdot\hat{d}_{nm}/d_{nm}]$ can be expanded in a Taylor series and only the lowest order terms retained. When this expression is placed in Eq. (26) and all the multipole terms higher than dipole-dipole terms are ignored, we find that

$$G_{mn}^{kj} \approx \frac{1}{4\pi\epsilon_b d_{nm}^3}[3(\mathbf{p}_m^k \cdot \hat{d}_{nm})(\mathbf{p}_n^j \cdot \hat{d}_{nm}) - \mathbf{p}_m^k \cdot \mathbf{p}_n^j]. \quad (29)$$

We recognize this expression as the interaction between two dipoles separated by a distance d_{nm}, where $\hat{d}_{nm}$ is the unit vector from particle m to particle n. This shows that the coupling G_{mn}^{kj} between two LSP modes is zero if the two modes have orthogonal dipole moments $\mathbf{p}_m^k \cdot \mathbf{p}_n^j = 0$ and if either of the modes is perpendicular to the direction of the line joining the two particles, $\mathbf{p}_m^k \cdot \hat{d}_{nm} = 0$ or $\mathbf{p}_n^j \cdot \hat{d}_{nm} = 0$. Equation (29) is very approximate in that it treats the interacting structures as point dipoles, which is never the case with interacting near fields. As such one would not use it to calculate the magnitude of the LSP coupling. However, it is useful in deciding whether or not two particles with LSPs will interact and whether or not that interaction is positive $G_{mn}^{kj} > 0$ or negative $G_{mn}^{kj} < 0$. Note that this coupling is symmetric under interchange of the nanoparticles: $G_{mn}^{kj} = G_{nm}^{jk}$. More generally we find that the coupling between particle pairs as described by Eq. (26) is symmetric unless the surface charge on one particle is concentrated at a point and the separation between particles is very small (Davis, Vernon, and Gómez, 2009a).

III. ANALYZING INTERACTIONS BETWEEN COUPLED LSPs

In this section we apply this theory to understand the interaction among ensembles of metal nanoparticles supporting localized surface plasmon resonances. There are four key equations that we use as follows:

(i) Eq. (7) for the LSP excitation of a single nanoparticle,
(ii) the approximate equation (9) for the resonance factor,
(iii) the matrix equation (28) linking the coupled excitations $\tilde{a}_n^j$ to the uncoupled excitations a_m^k, and
(iv) the dipole approximation (29) to estimate the sign of the coupling.

These equations reduce the coupling problem to relatively simple algebra. The resulting expressions can be analyzed to understand the effects of coupling and the functional forms of the LSP excitations can be graphed to understand the frequency dependence.

In all cases shown later, we assume each isolated nanoparticle has a single LSP resonance that dominates at the frequency of the incident light so that we need only consider one LSP mode on each particle. In this case we can drop the mode index, so that terms such as $G_{nm}^{11} \to G_{nm}$ and the equations are easier to follow. Also it is useful to write the denominator in Eq. (9) in short hand $\delta\tilde{\omega}_n = \omega - \omega_n + i\Gamma_n/2$ which saves us from writing out resonances and the FWHM until the end. In this shorthand notation, resonances occur when the real part $\mathrm{Re}\delta\tilde{\omega}_n = 0$ is zero. In solving coupling problems it is useful to have algebra manipulation software that can invert the matrix (28) algebraically. In our case we use the software DERIVE which is freely available.

A. Two particle coupling, dark modes, and Fano resonances

The simplest coupling problem is between two metal particles (Nordlander *et al.*, 2004). To emphasize that the theory is not restricted to regular shapes, such as rods, disks, or spheres, we show in Fig. 4(a) the lowest order resonances of two random-shaped metal nanostructures. Although the fundamental LSP modes may have a complicated multipole charge distribution, for very small structures the incident light couples predominantly to the dipole moments as discussed in

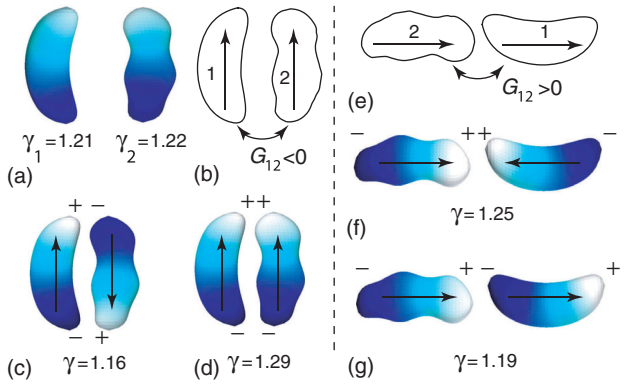

FIG. 4. An example of two coupled metal particles of arbitrary shape showing the formation of new resonant modes. (a) The first LSP modes of the two shapes and their eigenvalues, (b) a sketch used to calculate the side-by-side coupling, and (c) the "dark" mode as determined numerically. The arrows show the dipole moments; (d) the "bright" mode as determined numerically, (e) a sketch for end-to-end coupling, (f) the "dark" mode, and (g) the "bright" mode. The signs show the relative surface charges on each of the modes.

Sec. II. This fact allows us to write the interaction in terms of the dipole eigenfunctions.

To solve the coupling problem we number each nanostructure (in this case 1 and 2), sketch the dipole moments of the fundamental LSP modes (usually parallel to the major axis) as shown in Fig. 4(b), and write down the coupling between them. From Eq. (29) we note that the coupling $G_{12} = G_{21} < 0$ is negative so we write $G_{12} = G_{21} = -G$, where G is a positive quantity. Then, we apply Eq. (28) to form the *interaction matrix*

$$\begin{pmatrix} \tilde{a}_1 \\ \tilde{a}_2 \end{pmatrix} = \begin{pmatrix} 1 & -f_1 G_{12} \\ -f_2 G_{21} & 1 \end{pmatrix}^{-1} \begin{pmatrix} a_1 \\ a_2 \end{pmatrix} = \frac{1}{\Delta} \begin{pmatrix} 1 & f_1 G_{12} \\ f_2 G_{21} & 1 \end{pmatrix} \begin{pmatrix} a_1 \\ a_2 \end{pmatrix}. \tag{30}$$

The matrix inverse is easily found and has a determinant $\Delta = 1 - f_1 f_2 G^2$, where we make the substitution $G_{12} = G_{21} = -G$. The total dipole moment is given by $\mathbf{p} = \tilde{a}_1 \mathbf{p}_1 + \tilde{a}_2 \mathbf{p}_2$, where $\mathbf{p}_1$ and $\mathbf{p}_2$ are the eigenfunction dipole moments of the LSP modes.

For illustration purposes we assume the LSP dipole moments are the same $\mathbf{p}_1 = \mathbf{p}_2 = \mathbf{p}_{\mathrm{LSP}}$, that the loss terms are the same $\Gamma_1 = \Gamma_2 = \Gamma$, but the resonance frequencies differ by an amount 2δ so that $\omega_1 = \omega_{\mathrm{av}} - \delta$ and $\omega_2 = \omega_{\mathrm{av}} + \delta$, where ω_{av} is the average of the two resonance frequencies. Using the shorthand notation $\delta\tilde{\omega} = \omega - \omega_{\mathrm{av}} + i\Gamma/2$ then from Eq. (9) we can write $f_1 = -A/(\delta\tilde{\omega} + \delta)$, $f_2 = -A/(\delta\tilde{\omega} - \delta)$. With Eq. (7) we have the uncoupled amplitudes $a_1 = -A\mathbf{p}_{\mathrm{LSP}} \cdot \mathbf{E}_0/(\delta\tilde{\omega} + \delta)$ and $a_2 = -A\mathbf{p}_{\mathrm{LSP}} \cdot \mathbf{E}_0/(\delta\tilde{\omega} - \delta)$ and from the matrix equation (30) we can show that the amplitudes of the LSPs on each nanostructure are given by

$$\tilde{a}_1 = \frac{-A(\mathbf{p}_{\mathrm{LSP}} \cdot \mathbf{E}_0)(\delta\tilde{\omega} - \delta + AG)}{(\delta\tilde{\omega} - g)(\delta\tilde{\omega} + g)},$$
$$\tilde{a}_2 = \frac{-A(\mathbf{p}_{\mathrm{LSP}} \cdot \mathbf{E}_0)(\delta\tilde{\omega} + \delta + AG)}{(\delta\tilde{\omega} - g)(\delta\tilde{\omega} + g)}, \tag{31}$$

where $g = (\delta^2 + A^2G^2)^{1/2}$. The total dipole moment of the coupled pair is then

$$\mathbf{p} = \frac{-2A\mathbf{p}_{\mathrm{LSP}}(\mathbf{p}_{\mathrm{LSP}} \cdot \mathbf{E}_0)(\delta\tilde{\omega} + AG)}{(\delta\tilde{\omega} - g)(\delta\tilde{\omega} + g)}. \tag{32}$$

These equations show a number of important features found in coupled plasmonic systems. The easiest way to demonstrate these is to ignore the loss terms and set $\Gamma = 0$. Later we will include this again to plot the resonance spectra.

As an observation, note that the coupled amplitudes $\tilde{a}$ become large when the determinant Δ of the matrix in Eq. (30) becomes small. The condition that the real part of $\Delta = 0$ is zero generally determines the resonances of the coupled system. Moreover, the condition $\mathrm{Re}\Delta = 0$ can be expressed as a polynomial in frequency. The order of the polynomial determines the number of solutions, which then determines the number of resonances. For example, the determinant $\Delta = 1 - f_1 f_2 G^2$ from Eq. (30) has at most two solutions, so there are at most two resonances. In practice, as we show, it is possible for one or more of the zeros to cancel corresponding terms in the numerator. Such resonances are then virtual in that they cannot be excited and can be associated with dark modes.

1. Plasmon hybridization

We take the simple situation of two nanostructures with the same resonance frequencies whereby $\delta = 0$. If we look at the denominator in Eq. (31) or (32), we see that it becomes zero when $\mathrm{Re}\delta\tilde{\omega} = \pm|AG|$ or $\omega = \omega_R \pm |AG|$. In this case the single resonance ω_R splits into two resonances, with a splitting that depends on the strength of the coupling G. Such frequency splitting is a common feature of coupled oscillators.

In plasmonics literature, the formation of the new resonant modes, as in Figs. 4(c) and 4(d), and the associated frequency splitting is often referred to as *hybridization* (Prodan *et al.*, 2003; Nordlander *et al.*, 2004; Prodan and Nordlander, 2004), in analogy with the description of the nature of chemical bonds in terms of the superpositions of atomic orbitals. In both cases, the hybridization leads to an antisymmetric mode [Fig. 4(c)] and a symmetric mode [Fig. 4(d)]. The antisymmetric mode has opposite charges on the two metal structures facing each other, which is a lower energy configuration. The symmetric mode has the same charges facing one another creating a higher energy configuration. However, we note when $\delta = 0$, one of the resonance terms in the denominator of Eq. (32) cancels with a similar term in the numerator. When $G > 0$ the term responsible for the low frequency resonance cancels, $(\delta\tilde{\omega} + AG)/(\delta\tilde{\omega} + |AG|) = 1$. In this case the low frequency resonance, or antisymmetric mode, has a zero net dipole moment and will not radiate light. This is a *dark* mode that we examine in more detail later. The remaining *bright* mode has an energy that varies depending on the coupling. When $G < 0$, the high frequency resonance term cancels $(\delta\tilde{\omega} + AG)/(\delta\tilde{\omega} - |AG|) = 1$ leaving only the low frequency resonance, which is still a bright mode.

The sign of the coupling can change based on the relative orientations of the nanostructures. If we had allowed the orientations of the nanostructures in Fig. 4 to vary, so that $\mathbf{p}_n = p_{\mathrm{LSP}}(\cos\theta_n \hat{x} + \sin\theta_n \hat{y})$, then the coupling determined from Eq. (29) takes the form $G = -G_{12} \propto -3\cos\theta_1 \cos\theta_2 + \cos(\theta_2 - \theta_1)$, where $\hat{d}_{12} = \hat{x}$ and θ_1 is the angle nanostructure 1 takes with the x axis and likewise for θ_2 (Davis, Gómez, and Vernon, 2010c). In this situation the strength and sign of the coupling changes with the orientation of the nanostructures so that the energies, or resonance frequencies, of the hybrid modes change with orientation. For example, with $\theta_1 = \theta_2 = \pi/2$ as shown in Fig. 4(b), it is the high frequency resonance that is the bright mode [Fig. 4(d)]. In this case the LSP resonance has a higher energy because the resonant mode has charges of the same sign opposite one another. With $\theta_1 = \theta_2 = 0$ so that the nanostructures are aligned end to end [Fig. 4(e)], $G < 0$ and it is the low frequency resonance that is the bright mode [Fig. 4(g)] and the nanostructures have opposite charges facing one another, thus reducing the overall energy of the mode. The shifts in the plasmon resonances with coupling have been observed experimentally, with redshifts observed for end-to-end coupling (Haynes and Van Duyne, 2001; Rechberger *et al.*, 2003; Su *et al.*, 2003; Thaxton and

Mirkin, 2005; Jain, Eustis, and El-Sayed, 2006; Funston *et al.*, 2009) and blueshifts for side-by-side coupling (Rechberger *et al.*, 2003; Jain, Eustis, and El-Sayed, 2006; Funston *et al.*, 2009) consistent with our previous analysis.

2. Bright and dark modes

Suppose the coupling is strong so that $\delta \ll AG$ which implies that $g \approx AG$. At the low frequency resonance $\delta\tilde{\omega} = -g \approx -AG$ then the numerator of the LSP resonance $\tilde{a}_1$ in Eq. (31) is $\delta\tilde{\omega} - \delta + AG \approx -\delta$, whereas the numerator for particle 2 is $\delta\tilde{\omega} + \delta + AG \approx \delta$ which has the opposite sign to $\tilde{a}_1$. In effect, the direction of the dipole moment on one of the particles is opposite to the way we have drawn it for this LSP mode. This describes a resonance mode in which the LSPs on the two nanostructures have dipole moments pointing in opposite directions and therefore are oscillating 180° out of phase [Fig. 4(c)]. On the other hand, at the higher frequency resonance $\delta\tilde{\omega} = g \approx AG$ then both amplitudes have the same sign. For this resonance the LSPs oscillate in phase. This behavior agrees with the numerical simulation shown in Figs. 4(c) and 4(d). When we look at the total dipole moment we see that when $\delta\tilde{\omega} = -g \approx -AG$ the dipole moment Eq. (32) is zero so there is no radiation from the oscillating LSPs (when we include losses such that $\Gamma \neq 0$ there is a small residual dipole moment). This is a "dark mode" and is a consequence of the two LSPs oscillating out of phase. Provided $\delta \neq 0$ the incident light can excite this mode but there is little radiation from it and therefore little scattering and radiative damping.

3. Fano resonances

The total dipole moment of the coupled LSP system has a term in the numerator that is linearly dependent on the frequency, and its real part goes to zero at some frequency. This particular mathematical form is characteristic of a Fano resonance (Fano, 1961; Mirin, Bao, and Nordlander, 2009; Luk'yanchuk *et al.*, 2010; Miroshnichenko, Flach, and Kivshar, 2010). The Fano resonance arises from the interference between an incident wave and a wave scattered from a resonant object (Lovera *et al.*, 2013). There are three conditions for the phase at which a resonant object oscillates, depending on the frequency of the applied driving force: (1) It oscillates in phase with the driving force when driven well below its resonance frequency, (2) it oscillates 90° out of phase when resonantly driven, and (3) it oscillates 180° out of phase when driven well above resonance. If the resonance oscillation of the object is responsible for reemitting (or scattering) a wave, then the interference of the incident wave with the scattered one can alternate between destructive and constructive, resulting in a characteristic asymmetric resonance spectrum. This asymmetric Fano profile has the form $I = A_F(E_\omega + q)^2/(E_\omega^2 + 1)$, where q is a "shape factor" and E_ω represents a frequency-dependent normalized energy term. The line shape is asymmetric around a minimum, which occurs at a frequency $E_\omega = -q$ arising from the interference between two components of the system.

The intensity of the scattered radiation from the coupled nanorods is proportional to $|\mathbf{p}|^2$, which according to Eq. (32) has the approximate form of a Fano resonance (around the lower frequency resonance). Figure 5 shows a plot of the intensity, where the almost-dark mode demonstrates an asymmetric profile that can be fitted by the Fano equation. The Fano profile in this case arises from the interference of the radiation from two nanorods with different resonance frequencies, leading to constructive or destructive interference depending on the applied frequency.

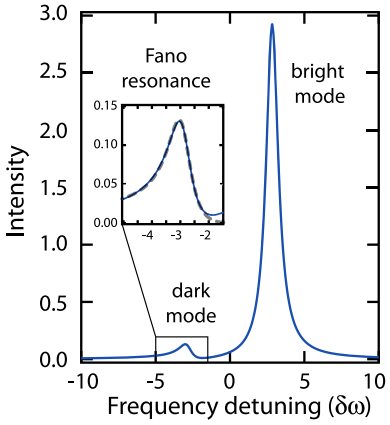

FIG. 5. A Fano resonance associated with two coupled metal particles. The intensity is calculated as a function of detuning $\delta\omega = \omega - \omega_R$ from the center resonance based on $|\mathbf{p}|^2$ from Eq. (32) with $|2A\mathbf{p}_1(\mathbf{p}_1 \cdot \mathbf{E}_0)| = 1$, $AG = 2$, $\Gamma = 1$, and $\delta = 2$. The inset shows the dark mode and the dashed curve is the Fano expression with the scaled energy term $E_\omega = 2(\delta\omega/\Gamma + 2.87)$, $q = -3.5$, and an amplitude scaling factor $A_F = 0.01$ [see the discussion of Miroshnichenko, Flach, and Kivshar (2010) around their Eq. (1)].

A more general description of Fano resonances in plasmonic nanostructures and metamaterials was presented by Gallinet and Martin (2011). In their approach, which is based on the formalism of Feshbach, Bhatia, and Temkin, the formal solutions to the full Maxwell equations are decomposed, or projected, into those which satisfy a radiation condition (bright modes) and those which do not (dark modes). The interaction of these two leads to the Fano line shape. Contrary to our approach, this treatment includes effects of radiative and nonradiative damping *ab initio* on the observed asymmetric line shapes.

B. Coupling in three nanorod structures

The LSP coupling between three nanorods provides an extraordinarily rich variety of optical behaviors. We begin by

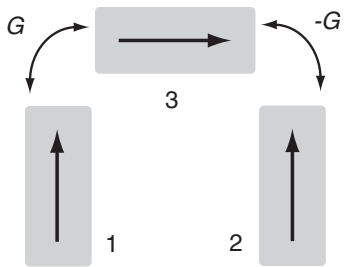

FIG. 6. A three-particle plasmonic structure, sometimes referred to as a "dolmen" structure, that mimics the Wheatstone bridge in electronics (Davis, Vernon, and Gómez, 2009a). The arrows represent the dipole moments of the fundamental LSP modes and G is the coupling coefficient.

analyzing a simple structure that demonstrates properties, such as induced transparency, phase sensitivity, all-optical modulation and switching, and then discuss a radially symmetric structure with radial dark modes.

We consider a set of three nanorods forming a "dolmenlike" structure shown in Fig. 6. We assume the two parallel nanorods are sufficiently far apart so that the interaction between them is dominated by their coupling to nanorod 3. We also assume that all three nanorods are identical and therefore have the same LSP resonance frequency ω_R, loss terms Γ, and eigenfunction dipole moments $|\mathbf{p}_1| = |\mathbf{p}_2| = |\mathbf{p}_3|$, where we assume one dominant LSP mode on each and drop the mode superscript. Under these conditions, Eq. (28) describing the excitation amplitudes for these coupled nanorods is given by

$$\begin{pmatrix} \tilde{a}_1 \\ \tilde{a}_2 \\ \tilde{a}_3 \end{pmatrix} = \begin{pmatrix} 1 & 0 & -fG \\ 0 & 1 & fG \\ -fG & fG & 1 \end{pmatrix}^{-1} \begin{pmatrix} a_1 \\ a_2 \\ a_3 \end{pmatrix} = \frac{1}{\Delta} \begin{pmatrix} 1-f^2G^2 & -f^2G^2 & fG \\ -f^2G^2 & 1-f^2G^2 & -fG \\ fG & -fG & 1 \end{pmatrix} \begin{pmatrix} a_1 \\ a_2 \\ a_3 \end{pmatrix}, \quad (33)$$

where $G > 0$ represents the coupling between the particles and $\Delta = 1 - 2f^2G^2$ is the matrix determinant. Having inverted the matrix we obtain in just a few lines of algebra the fundamental equations that describe the interactions among these three nanorods and an incident field, as we now proceed to illustrate.

1. Plasmon-induced transparency

For this example the incident light is polarized parallel to nanorod 3 so that $a_1 = a_2 = 0$ [this also mimics the experimental conditions of Liu *et al.* (2009)]. With Eq. (33), it is straightforward to show that $\tilde{a}_1 = fG\tilde{a}_3$ and $\tilde{a}_2 = -fG\tilde{a}_3$; that is, these two rods oscillate out of phase with each other resembling a collective quadrupole (dark) mode (Liu *et al.*, 2009). Since $\tilde{a}_1 + \tilde{a}_2 = 0$, the total dipole moment in the polarization along these two rods vanishes, and this reduces radiative damping, as in Eq. (20).

The light scattered from nanoparticle 3 is described by the excitation amplitude $\tilde{a}_3$, which according to Eq. (33) is given by $\tilde{a}_3 = a_3/(1-2f^2G^2)$. Using the shorthand notation $\delta\tilde{\omega} = \omega - \omega_R + i\Gamma/2$, we write $a_3 = -A\mathbf{p}_3 \cdot \mathbf{E}_0/\delta\tilde{\omega}$ and $f = -A/\delta\tilde{\omega}$ which leads to

$$\tilde{a}_3 = \frac{-A(\mathbf{p}_3 \cdot \mathbf{E}_0)\delta\tilde{\omega}}{(\delta\tilde{\omega} - \sqrt{2}AG)(\delta\tilde{\omega} + \sqrt{2}AG)}. \quad (34)$$

We immediately see that the coupling of nanorod 3 to the two parallel nanorods leads to a resonance splitting that depends on the coupling strength G. The two new resonances occur at frequencies $\omega_\pm$ for which the denominator of Eq. (34) is zero, that is when $(\delta\tilde{\omega})^2 - 2(AG)^2 = 0$. For weak coupling, $G \approx 0$ there is only one resonance that occurs at ω_R (the resonance frequency of the individual particle). As the coupling increases, the resonances $\omega_\pm$ move apart (Fig. 7), and the magnitude of the excitation amplitude $\tilde{a}_3$ decreases significantly at zero detuning (i.e., when the real part of $\delta\tilde{\omega} = 0$). This strong drop in the excitation amplitude leads to a dramatically reduced scattering of the light at the frequency of the isolated nanoparticle (ω_R), which is experimentally observable as an increase in the transparency of an array of such structures (Liu *et al.*, 2009; Hokari, Kanamori, and Hane, 2014). This effect has been termed plasmon-induced "transparency" (Zhang *et al.*, 2008) and is related to the splitting of the resonances due to coupling. If we had included the radiation damping in Fig. 7, then the width of the transparency region would be narrower than shown, due to the reduced damping associated with the quadrupole.

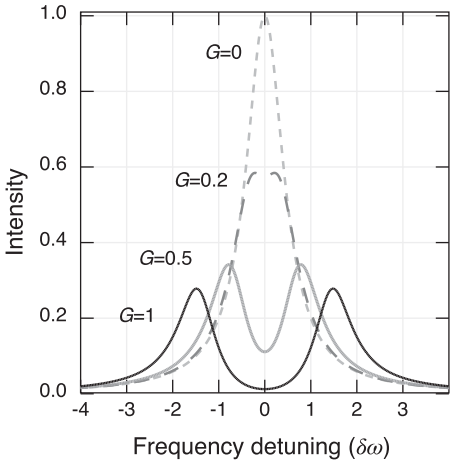

FIG. 7. The spectrum of a three-particle configuration that demonstrates the formation of induced transparency at zero detuning $\delta\omega = \omega - \omega_R$ as the coupling strength G increases. The spectra are based on $|\tilde{a}_3|^2$ calculated from Eq. (34) with $\Gamma = 1$, $A = 1$, and $\mathbf{p}_3 \cdot \mathbf{E}_0 = 0.5$.

2. Plasmonic Wheatstone bridge

Suppose instead we excite the structure in Fig. 6 with light polarized parallel to the two nanorods (1 and 2) and perpendicular to the third. However, we place a polarizer at the output that accepts only light radiated from nanorod 3. In this case $a_1 \neq 0$ and $a_2 \neq 0$ but $a_3 = 0$ and according to Eq. (33), the output $\tilde{a}_3 = fG(a_1 - a_2)/(1-2f^2G^2)$ now depends on the difference of the LSP excitations on the two parallel nanorods. Let the light be incident at some angle so there is a phase difference between the excitations on nanorods 1 and 2. That is, let $a_1 = -A\mathbf{p}_3 \cdot \mathbf{E}_0 \exp(i\phi/2)/\delta\tilde{\omega}$ and $a_2 = -A\mathbf{p}_3 \cdot \mathbf{E}_0 \exp(-i\phi/2)/\delta\tilde{\omega}$, then the LSP excited in nanorod 3 is given by

$$\tilde{a}_3 = \frac{2i\sin(\phi/2)A^2G(\mathbf{p}_3 \cdot \mathbf{E}_0)}{(\delta\tilde{\omega} - \sqrt{2}AG)(\delta\tilde{\omega} + \sqrt{2}AG)}. \quad (35)$$

The structure produces an LSP in the third rod with an amplitude that depends on the *phase difference* ϕ of the light incident on the two parallel rods. The configuration leads to the interference between the two surface plasmons on the parallel rods and, in effect, performs a mathematical difference operation on them. This configuration is analogous to the Wheatstone bridge circuit in electronics (Davis, Vernon, and Gómez, 2009) that generates a signal between its two arms when they are imbalanced. Nanorod 3 plays the role of the volt meter that reads out the difference signal. Such structures can be extremely small and can probe an optical phase within a fraction of a wavelength (Eftekhari, Gómez, and Davis, 2014), as shown in Fig. 8. The

intensity of the scattered light is proportional to $|\tilde{a}_3|^2$, which varies with phase as $\sin^2(\phi/2) \approx \phi^2/4$. This variation is quadratic in phase for small phase differences, in agreement with the experimental results.

3. All-optical modulation

In the last section we used an analogy between metal particles coupled by evanescent fields and an electric circuit operating at optical frequencies. This concept has been applied for some time to plasmonic structures, since the LSP resonance can be modeled by a combination of an inductor, capacitor, and a resistor (Engheta, Salandrino, and Alù, 2005; Engheta, 2007; Davis, Vernon, and Gómez, 2009; Sun *et al.*, 2012; Liu *et al.*, 2013; Abasahl, Santschi, and Martin, 2014). Electrical circuits made from these components are linear, which means the circuit can be driven in reverse: that is, the outputs can be driven by a signal and an inverse response observed at the inputs. Since the plasmonic circuit in the previous example produces an output depending on the phase at the inputs, it should be possible to drive the output with an intensity that modulates the phase at the inputs. In this final example using the same three-nanostructure configuration, we show that indeed this is possible by analyzing what happens when light is incident on all three nanorods.

It is convenient to explicitly show the phases of all quantities. We express the resonance factor as a magnitude f_ω and a phase ϕ_w such that $f(\omega) = f_\omega e^{i\phi_\omega}$. Light is incident at some angle on two identical rods 1 and 2 lying in the x-y plane at $z = 0$ [Fig. 9(a)]. The light is polarized parallel to their long axes so that it does not excite rod 3 (see Fig. 6). In this configuration we assume there is a polarizer on the output that passes light scattered only from rods 1 and 2. With $\mathbf{k}_I$ the incident wave vector, there is a phase difference between the LSP excitations related to the vector separation $\mathbf{d}$. The phase difference is $e^{\mp i\mathbf{k}_I\cdot\mathbf{d}/2}$. Likewise, light radiated from these rods in the same direction $\mathbf{k}_I$ has the opposite phase difference $e^{\pm i\mathbf{k}_I\cdot\mathbf{d}/2}$. Since the rods are identical, we can write

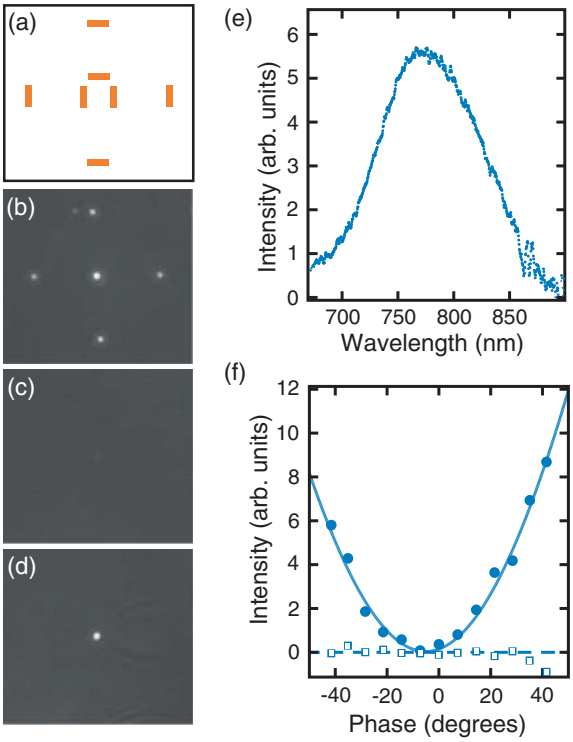

FIG. 8. Results of experiments on a single plasmonic Wheatstone bridge circuit. (a) A schematic diagram of the configuration of nanorods, including four alignment rods used to ensure correct alignment of polarizers; (b) a microscope image showing light scattered from the circuit and the four alignment nanorods; (c) the scattering intensity obtained with the substrate correctly aligned and with normal incident light (zero phase difference); (d) with light incident at $\theta = 30°$ the circuit appears as a bright spot at the center of the image; (e) scattering spectrum from the plasmonic circuit; and (f) the intensity as a function of phase difference between the two inputs (dots are experimental data, the solid curve is theory). Also shown is the null response of the circuit (square points) where the phase change is between the parallel rods and rod 3. The dashed line is the expected response in the null orientation. Adapted from Eftekhari, Gómez, and Davis, 2014.

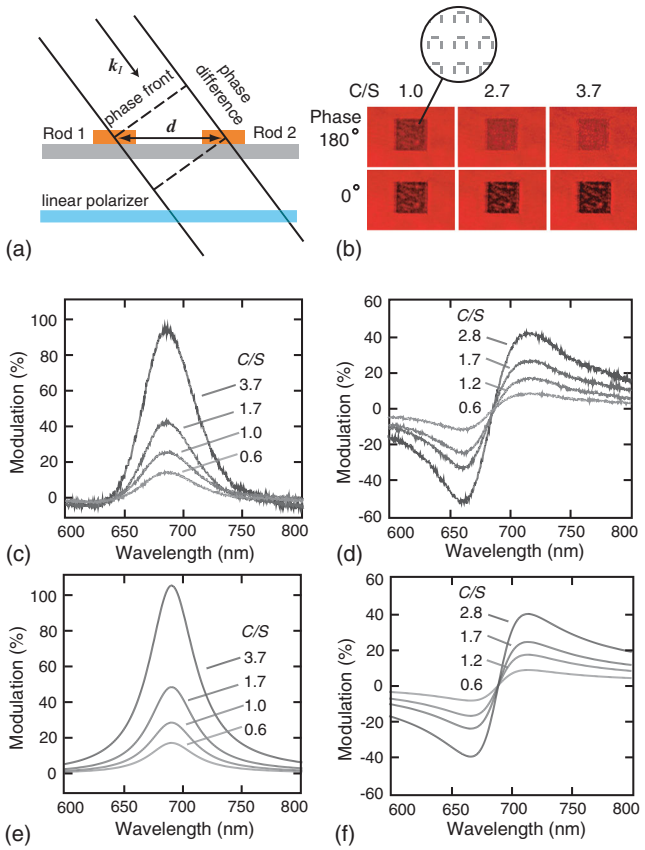

FIG. 9. A plasmonic all-optical modulator. A metamaterial can be created with arrayed plasmonic Wheatstone-bridge circuits (based on the diagram of Fig. 6) where a signal S and a control C beam are orthogonally polarized. (a) Diagram showing the phase difference of LSP excitation on rods 1 and 2 on a substrate arising from a light beam incident at an angle; (b) images of the transmission through arrays of plasmonic circuits for different ratios C/S and phases ϕ_c, showing the modulation effect; (c), (d) experimental measurements of the modulation determined for changes in phase (c) $\phi_c = 0° \to 180°$ (d) $\phi_c = -90° \to 90°$; and (e), (f) the corresponding theoretical modulation based on Eq. (39). Adapted from Davis, Gómez, and Eftekhari, 2014.

$a_1 = f_\omega S e^{-i\mathbf{k}_I\cdot\mathbf{d}/2+i\phi_\omega}$ and $a_2 = f_\omega S e^{i\mathbf{k}_I\cdot\mathbf{d}/2+i\phi_\omega}$, where S is proportional to the amplitude of the incident light.

There is also a second light beam incident that is polarized so that it induces only LSPs in rod 3. We impose a phase ϕ_c on this beam relative to the light incident on rods 1 and 2. Then $a_3 = f_\omega C e^{i\phi_c+i\phi_\omega}$ where C is proportional to the amplitude of the light. As a further approximation, we assume the coupling G is small enough that we can neglect terms G^2 and those of higher order. Then the amplitudes of the LSPs in rods 1 and 2 are obtained from the coupling matrix (33)

$$\tilde{a}_1 \approx f_\omega e^{i\phi_\omega}(Se^{-i\mathbf{k}_I\cdot\mathbf{d}/2} + GCf_\omega e^{i\phi_c+i\phi_\omega}),$$
$$\tilde{a}_2 \approx f_\omega e^{i\phi_\omega}(Se^{i\mathbf{k}_I\cdot\mathbf{d}/2} - GCf_\omega e^{i\phi_c+i\phi_\omega}). \quad (36)$$

Taking account of the fact that the two rods are separated by a small distance, then the scattered wave amplitude in direction $\mathbf{k}_I$ is

$$\tilde{a}_T = \tilde{a}_1 e^{i\mathbf{k}_I\cdot\mathbf{d}/2} + \tilde{a}_2 e^{-i\mathbf{k}_I\cdot\mathbf{d}/2}$$
$$\approx 2f_\omega e^{i\phi_\omega}[S + iGCf_\omega e^{i\phi_c+i\phi_\omega}\sin(\mathbf{k}_I\cdot\mathbf{d}/2)], \quad (37)$$

where any scattering from rod 3 is filtered out by a polarizer. The intensity of the scattered wave is related to $I = |\tilde{a}_T|^2$ which is

$$I = 4f_\omega^2[S^2 - 2f_\omega GCS\sin(\mathbf{k}_I\cdot\mathbf{d}/2)\sin(\phi_c+\phi_\omega)$$
$$+ f_\omega^2 G^2C^2\sin^2(\mathbf{k}_I\cdot\mathbf{d}/2)]. \quad (38)$$

This equation shows the intensity I of the beam scattered by an array of such structures modulated by the amplitude C and phase ϕ_c of a beam of light incident on rod 3, even though this beam is filtered out by the polarizer and does not reach the detector. The modulation arises due to interference between the LSPs created in the coupled structure by the two light beams.

The optical modulation strength M can be defined as the difference of the intensity of the transmitted light when the phase is shifted from ϕ_c to $\phi_c + 180°$, divided by the intensity $4f_\omega^2 S^2$ of the beam scattered directly by rods 1 and 2. This gives

$$M = 4f_\omega G(C/S)\sin(\mathbf{k}_I\cdot\mathbf{d}/2)\sin(\phi_c+\phi_\omega). \quad (39)$$

In Fig. 9(b) we show an experimental demonstration of this all-optical modulation with a metamaterial created from an array of plasmonic Wheatstone-bridge circuits of Fig. 6 (Davis, Gómez, and Eftekhari, 2014). The transmission through the metamaterial changes when either the amplitude or phase of the "control" beam exciting nanorod 3 is varied. The experimentally measured modulations as functions of wavelength and control beam parameters are compared in Figs. 9(c)–9(f) with calculations based on Eq. (39). The resonance factor is given by $f_\omega = A/(\delta\omega^2 + \Gamma^2/4)$ and $\tan\phi_\omega = -\Gamma/2\delta\omega$. The resonance frequency and width used in the calculation was obtained from the experimental data and the unknown scale factors $4AG$ were found by matching the modulation in Fig. 9(f) to the experimental value at $C/S = 1.2$ and $\lambda = 715$ nm. No other scaling was applied. Despite the complexity of this configuration and experiment, Eq. (39) shows remarkable agreement with experiment, which highlights the predictive power of this simple coupling theory, despite the approximations that have been used in deriving it.

All-optical modulation in this structure originates by interfering the polarized incident beam with another beam having orthogonal polarization, in such a way that the second beam is unable to propagate through the metamaterial effectively. In one sense, the beam incident on nanorod 3 excites LSPs on nanorods 1 and 2 that oscillate 180° out of phase with each other and therefore the beams scattered from these rods cancel out. However, the beam coupling from rod 3 interferes with the incident light scattered from rods 1 and 2 leading to a decrease in intensity. This can be thought of as a subwavelength interferometer. By making a diffraction grating based on these structures it is possible to create an *all-optical switch*, or a diffraction grating with an *optically controlled blaze* (Davis, Gómez, and Eftekhari, 2014).

4. Radially symmetric structures and dark modes

Here we consider another three nanorod structure, one that exhibits radially symmetric dark modes, that we analyze using the theory developed in Sec. II (Gómez *et al.*, 2013).

To describe the interaction of light with the structure shown in Fig. 10, we use Eq. (28) to find the excitation amplitudes under the assumption that all the particles are identical and equidistant. The matrix equation is (Gómez *et al.*, 2013)

$$\begin{pmatrix}\tilde{a}_1\\ \tilde{a}_2\\ \tilde{a}_3\end{pmatrix} = \begin{pmatrix}1 & -fG & -fG\\ -fG & 1 & -fG\\ -fG & -fG & 1\end{pmatrix}^{-1}\begin{pmatrix}a_1\\ a_2\\ a_3\end{pmatrix}$$
$$= \frac{1}{\Delta}\begin{pmatrix}1-f^2G^2 & f^2G^2+fG & f^2G^2+fG\\ f^2G^2+fG & 1-f^2G^2 & f^2G^2+fG\\ f^2G^2+fG & f^2G^2+fG & 1-f^2G^2\end{pmatrix}$$
$$\times\begin{pmatrix}a_1\\ a_2\\ a_3\end{pmatrix}, \quad (40)$$

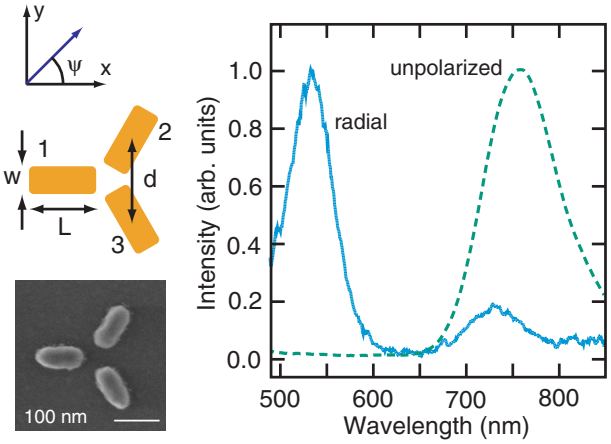

FIG. 10. Radially symmetric trimer exhibiting a radial dark mode. Experimentally measured spectra for unpolarized and radially polarized light incident on a gold single trimer, shown in the scanning electron micrograph (SEM) on the left. Adapted from Gómez *et al.*, 2013.

where the determinant $\Delta = 1 - 2(fG)^3 - 3(fG)^2$ is of the order of 3 in f, which implies that the structure has three collective resonances.

To proceed further, we write the incident electric field $\mathbf{E}_0$ as a superposition of a linearly polarized component with amplitude E_l and a radially polarized one with amplitude E_r: $\mathbf{E}_0 = E_l(\cos\psi\hat{x} + \sin\psi\hat{y}) + E_r\hat{r}$, where $\hat{r}$ is a unit vector pointing radially outward from the origin of coordinates and ψ is the angle that the linearly polarized component subtends with respect to the horizontal. This is an approximate way to describe a field with radial symmetry. Accurate descriptions are more complicated as shown in the literature (Mojarad and Agio, 2009; Sancho-Parramon and Bosch, 2012). However, this simplistic approach allows us to extract physically relevant information that closely reproduces the experimental observations.

For the case of incident radial polarization ($E_l = 0$), straightforward (but lengthy) algebraic manipulation of Eq. (40) yields equal excitation amplitudes for all three nanorods, given by

$$\tilde{a} = \frac{AE_r p}{\delta\tilde{\omega} - 2AG}, \tag{41}$$

which predicts the excitation of a radially symmetric mode with net zero dipole moment and a resonance frequency given by the real part of $\omega_d = \omega_R + 2AG$.

For the case of linearly polarized light ($E_r = 0$) incident with a polarization angle ψ as shown in Fig. 10, the excitation amplitudes are given by

$$\begin{aligned}
\tilde{a}_1 &= -\frac{AE_l p}{AG + \delta\tilde{\omega}}\cos\psi, \\
\tilde{a}_2 &= \frac{AE_l p}{AG + \delta\tilde{\omega}}\frac{1}{2}(\sqrt{3}\sin\psi + \cos\psi), \\
\tilde{a}_2 &= \frac{AE_l p}{AG + \delta\tilde{\omega}}\frac{1}{2}(\cos\psi - \sqrt{3}\sin\psi),
\end{aligned} \tag{42}$$

and therefore the total dipole moment $\mathbf{p} = \sum_n \tilde{a}_n \vec{p}_n$ is

$$\mathbf{p}_l = -\frac{3AE_l p^2}{2(AG + \delta\tilde{\omega})}(\cos\psi\hat{x} + \sin\psi\hat{y}). \tag{43}$$

This equation represents a bright plasmon mode, with a doubly degenerate resonance frequency $\omega_b = \omega_R - AG$ red-shifted from the plasmon resonance of the individual nanorods.

The line shape of the scattering spectrum of this D_{3h}-symmetric trimer is proportional to $|\mathbf{p}|^2$, which according to Eq. (43) results in a single scattering band centered at the resonance frequency of the doubly degenerate bright modes. According to Eq. (41), the dark mode can be excited by a radially polarized beam of light (i.e., it can absorb), but by virtue of not having a net dipole moment, the absence of radiative damping leads to a narrower line shape when compared to the bright mode [compare with Eq. (19)]. These predictions were experimentally confirmed by Gómez *et al.* (2013) and summarized in Fig. 10 demonstrating here the predicting power of the analytic theory of Sec. II.

C. Coupling in 3D structures

We have shown the applicability of the theory developed in Sec. II to LSP coupling between two particles and among three particles. We now turn our attention to a special case consisting of the three-dimensional arrangement of Fig. 11, called the *three-dimensional plasmonic ruler*, a concept first introduced by Liu *et al.* (2011). This structure contains two vertically displaced metal nanorod dimers (aligned side to side) and a fifth nanorod, placed centrally at a right angle with respect to the dimers.

The symmetry of the three-dimensional plasmon ruler allows for significant simplifications of Eq. (28). For instance, the LSP coupling in each nanorod pair can be described with a single coupling constant, which for brevity we denote as $C_{nm} \equiv f_n G_{nm}$ (where n and m are particle indices). These pairs are not mutually coupled (by virtue of their long vertical separation distance), implying there are two 2×2 blocks describing LSP coupling for each pair and two 2×2 off-diagonal blocks containing only zeros. Coupling between the central rod and the lower pair of nanorods is approximately equal but opposite, $C_{a1} = -C_{a2}$. Similar considerations for the remaining interactions involving the central rod lead to the following form for Eq. (28):

$$\begin{pmatrix} \tilde{a}_a \\ \tilde{a}_1 \\ \tilde{a}_2 \\ \tilde{a}_3 \\ \tilde{a}_4 \end{pmatrix} = \begin{pmatrix} 1 & -C_{a1} & C_{a1} & -C_{a3} & C_{a3} \\ -C_{a1} & 1 & -C_{12} & 0 & 0 \\ C_{1a} & -C_{12} & 1 & 0 & 0 \\ -C_{3a} & 0 & 0 & 1 & -C_{34} \\ C_{3a} & 0 & 0 & -C_{34} & 1 \end{pmatrix}^{-1} \times \begin{pmatrix} a_a \\ a_1 \\ a_2 \\ a_3 \\ a_4 \end{pmatrix}. \tag{44}$$

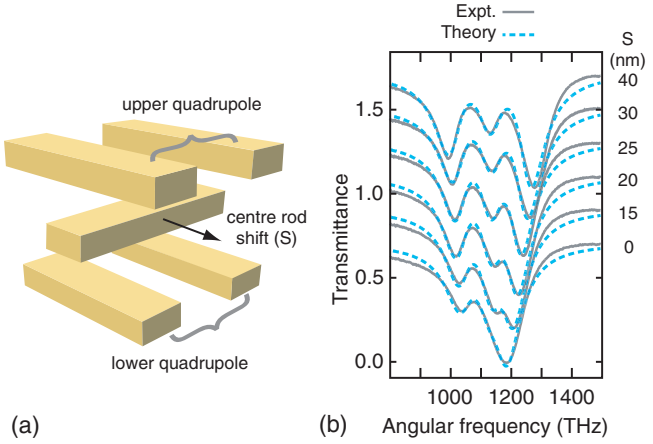

FIG. 11. Three-dimensional plasmonic ruler. (a) A sketch of the ruler: the upper and lower quadrupoles are created by LSP dipole modes excited in opposite directions in each pair of rods due to coupling from the central rod, and (b) experimental data from Liu *et al.* (2011) and the analytical model fitted to the data for different lateral translations S of the central rod. Adapted from Davis *et al.*, 2012.

The determinant of the matrix, required for the matrix inverse, is given by

$$\Delta = \frac{2G_{al}^2}{\omega - \omega_{ql} + i\Gamma/2} + \frac{2G_{au}^2}{\omega - \omega_{qu} + i\Gamma/2} - (\omega - \omega_a + i\Gamma/2), \tag{45}$$

where $\omega_{ql} = \omega_l + G_l$ is the quadrupole resonance associated with the coupling G_l between the lower pair of nanorods, and likewise $\omega_{qu} = \omega_u + G_u$ is the quadrupole resonance for the upper pair. The transmission spectrum is proportional to $I_{\max} - A_a^2/|\Delta|^2$ so that the maxima and minima in the determinant Δ control the respective minima and maxima in the transmission spectrum. As shown in Fig. 11(b) this expression fits the experimental data very well. A further analysis of the determinant yields an approximate expression for the resonance frequencies that enables identification of the key factors that control each feature in the scattering spectrum (Davis *et al.*, 2012).

IV. CONCLUDING REMARKS

As we have shown, a simple algebra based on the electrostatic eigenmode theory is capable of providing useful physical insights into the optical properties of ensembles of metal particles exhibiting localized surface plasmon resonances. It can, furthermore, be used to describe the interaction of metal nanoparticles with single molecules (Davis, Gómez, and Vernon, 2010a, 2010b; Gómez *et al.*, 2012) and chiral media (Davis and Gómez, 2014). The algebra is derived from the electrodynamics of piecewise continuous dielectric media and consequently does not account for nonlocal and quantum mechanical effects that have been argued to take place at interparticle separation distances of less than 1 nm (Savage *et al.*, 2012; Zhu *et al.*, 2016).

Nevertheless, the method appears to encompass most of the important physics associated with interacting metal particles and is capable of predicting the important features and behaviors of LSP spectra. Moreover, if experimental values are used for the linewidths and resonance frequencies, the electrostatic algebraic method gives quite accurate predictions of the optical effects of LSP coupling in nanoparticle ensembles.

ACKNOWLEDGMENTS

The authors acknowledge support from the Australian Research Council Discovery Project No. DP160100983, the Future Fellowship No. FT140100514, the Veski Victoria Fellowship, and the Melbourne Centre for Nanofabrication (MCN) in the Victorian Node of the Australian National Fabrication Facility (ANFF).

APPENDIX A: THE EIGENMODES AND EIGENVALUES OF EQ. (4) FOR A SPHERE

We illustrate the application of Eq. (4) for the analytical description of a metallic nanosphere in terms of eigenmodes and its interaction with an external electric field. Some of the results found in this section have also been applied for describing the interaction of molecules with metal nanoparticles (Davis, Gómez, and Vernon, 2010b).

The starting point is to expand the surface charge density using the spherical harmonics as a basis set (Jackson, 1975):

$$\sigma(\mathbf{r}) = \sum_{k,n} \sigma_{k,n}(R) Y_{k,n}(\Omega), \tag{A1}$$

where $\Omega = \theta, \phi$ denotes the solid angle in the sphere which is considered to have a radius R. $\sigma_{k,n}(R) = A_{k,n}R^k + B_{k,n}R^{-(k+1)}$ is the radial part with coefficients as yet undetermined and the second index in the summation $n = -k, -|k-1|, \ldots, 0, \ldots, k-1, k$.

Equation (4) can also be expressed as

$$\sigma(\mathbf{r}) = -\frac{\gamma}{2\pi} \oint \sigma(\mathbf{r}')\hat{n} \cdot \boldsymbol{\nabla} \frac{1}{|\mathbf{r} - \mathbf{r}'|} dS', \tag{A2}$$

and the term $1/|\mathbf{r} - \mathbf{r}'|$ can be expanded using spherical harmonics using the well-known expression (Jackson, 1975):

$$\frac{1}{|\mathbf{r} - \mathbf{r}'|} = 4\pi \sum_{l,m} \frac{1}{2l+1} \frac{r_<^l}{r_>^{l+1}} Y_{l,m}^*(\Omega') Y_{l,m}(\Omega). \tag{A3}$$

Substituting this and Eq. (A1) into Eq. (A2):

$$\begin{aligned}
\sigma(\mathbf{r}) &= -\frac{\gamma}{2\pi} \sum_{k,n} \sum_{l,m} \frac{4\pi}{2l+1} \int_0^{2\pi} d\phi' \\
&\quad \times \int_0^{\pi} d\theta' \sin(\theta') Y_{l,m}^*(\Omega') Y_{l,m}(\Omega) Y_{k,n}(\Omega') \\
&\quad \times R^2 \sigma_{k,n}(R) \hat{n} \cdot \boldsymbol{\nabla} \frac{r_<^l}{r_>^{l+1}} \\
&= \frac{\gamma}{2\pi} \sum_{k,n} \sum_{l,m} \frac{4\pi}{2l+1} \delta_{k,l} \delta_{n,m} R^2 \sigma_{k,n}(R) \frac{1}{2R^2} \\
&= \frac{\gamma}{2k+1} \sum_{k,n} \sigma_{k,n}(R) Y_{k,n}(\Omega),
\end{aligned} \tag{A4}$$

which according to Eq. (A1) imply that the eigenvalues γ are thus

$$\gamma = 2k + 1. \tag{A5}$$

A requirement of charge neutrality for the surface charge distribution reads

$$\begin{aligned}
\oint \sigma(\mathbf{r}) dS = 0 &= \sum_{l,m} \int_0^{2\pi} d\phi \int_0^{\pi} d\theta \sin(\theta) R^2 \sigma_{l,m}(R) Y_{l,m}(\Omega) \\
&= \sum_{l,m} \int_0^{2\pi} d\phi \int_0^{\pi} d\theta \sin(\theta) Y_{l,m}(\Omega) Y_{0,0}(\Omega) \\
&\quad \times R^2 \sigma_{l,m}(R) \sqrt{4\pi} \\
&= \sum_{l,m} \delta_{l,0} \delta_{m,0} R^2 \sigma_{l,m}(R) \sqrt{4\pi},
\end{aligned} \tag{A6}$$

a condition satisfied only if $\sigma_{0,0}(R) = 0$, i.e., the expansion of Eq. (A1) is made only for $k > 0$. Therefore, for a spherical object, the eigenmodes of Eq. (4) are $\sigma_{k,n}(R) Y_{k,n}(\Omega)$ with

eigenvalues $2k+1$ (each being $2k+1$ degenerate) where the index $k = 1, 2, \ldots$.

The solutions to Eq. (6) can also be found by following the same procedure. However, as stated in Sec. II, the solutions to Eqs. (4) and (6) form a biorthogonal set, for which $\oint \tau_m^i(\mathbf{r})\sigma_n^j(\mathbf{r})dS = \delta_{mn}\delta^{ij}$, requiring that the functional form of $\tau_m^i(\mathbf{r})$ is $\tau_m^i(\mathbf{r}) = \tau_m^i(R)Y_{ml}^*(\Omega)$ (with $l = -m, -|m-1|, \ldots, 0, \ldots, m-1, m$):

$$\begin{aligned}\delta_{mn}\delta^{ij} &= \oint \tau_m^i(\mathbf{r})\sigma_n^j(\mathbf{r})dS \\ &= \int_0^{2\pi} d\phi \int_0^{\pi} d\theta \sin(\theta) R^2 \tau_m^i(R)\sigma_n^j(R)Y_{ml}^*(\Omega)Y_{nk}(\Omega) \\ &= R^2\tau_m^i(R)\sigma_n^j(R)\delta_{mn}\delta_{lk}, \end{aligned} \tag{A7}$$

which imply thus $\delta^{ij} = R^2\tau_m^i(R)\sigma_m^j(R)$.

We now proceed to analyze the interaction of a metal sphere with a uniform incident electric field, polarized along the $\hat{z}$ axis. Because of this interaction, the sphere will support an LSP described by a superposition of eigenmodes $\sigma(\vec{r}) = \sum_m a_m(\omega)\sigma_m(\mathbf{r})$, where the excitation amplitude $a_m(\omega)$ of the mth eigenmode is given by Eq. (7) of Sec. II:

$$\begin{aligned} a_m(\omega) &= f_m(\omega) \oint \tau_m(\mathbf{r})\hat{n}\cdot\mathbf{E}_0(\mathbf{r})dS \\ &= f_m(\omega) \oint \tau_m(\mathbf{r})E_0\cos(\theta)dS \\ &= \sum_{l=-m}^{m} f_m(\omega)E_0\sqrt{\frac{4\pi}{3}}\int_0^{2\pi}d\phi\int_0^{\pi}d\theta\sin(\theta) \\ &\quad \times R^2\tau_m(R)Y_{ml}^*(\Omega)Y_{1,0}(\Omega) \\ &= f_m(\omega)E_0\sqrt{\frac{4\pi}{3}}R^2\tau_m(R)\delta_{m1}\delta_{l0} \end{aligned} \tag{A8}$$

meaning that under this illumination, the surface charge distribution describing the sphere's LSP is

$$\begin{aligned}\sigma(\mathbf{r}) &= \sum_m f_m(\omega)E_0\sqrt{\frac{4\pi}{3}}R^2\tau_m(R)\sigma_m(R)Y_{ml}(\Omega)\delta_{m1}\delta_{l0} \\ &= f_{m=1}(\omega)E_0\sqrt{\frac{4\pi}{3}}Y_{10}(\Omega) \\ &= \frac{3\epsilon_b(\epsilon_m(\omega)-\epsilon_b)}{2\epsilon_b+\epsilon_m(\omega)}E_0\sqrt{\frac{4\pi}{3}}Y_{10}(\Omega), \end{aligned} \tag{A9}$$

which is the result found by directly solving the Laplace equation in spherical coordinates (Böttcher *et al.*, 1978).

The dipole moment $\mathbf{p}$ associated with this charge distribution is found by performing the surface integral $\oint \sigma(\mathbf{r})\mathbf{r}dS$, recognizing that $\mathbf{r} = r[\sin(\theta)\cos(\phi)\hat{x} + \sin(\theta)\sin(\phi)\hat{y} + \cos(\theta)\hat{z}]$:

$$\begin{aligned}\mathbf{p} &= a_{m=1}(\omega)\oint \sigma_{m=1}(R)Y_{10}(\Omega)\mathbf{r}dS \\ &= a_{m=1}(\omega)\int_0^{2\pi}d\phi\int_0^{\pi}d\theta\sin(\theta)Y_{10}(\Omega)Y_{10}(\Omega) \\ &\quad \times R^3\sigma_{m=1}(R)\sqrt{\frac{4\pi}{3}}\hat{z} \\ &= a_{m=1}(\omega)R^3\sigma_{m=1}(R)\sqrt{\frac{4\pi}{3}}\hat{z} \end{aligned} \tag{A10}$$

and substitution of the expression for the excitation amplitude, bearing in mind the biorthogonality condition:

$$\begin{aligned}\mathbf{p} &= \frac{4\pi R^3}{3}f_{m=1}(\omega)E_0[R^2\tau_1(R)\sigma_1(R)]\hat{z} \\ &= \frac{3\epsilon_b[\epsilon_m(\omega)-\epsilon_b]}{2\epsilon_b+\epsilon_m(\omega)}\frac{4\pi R^3}{3}E_0\hat{z}, \end{aligned} \tag{A11}$$

which is also in agreement with well-known results (Böttcher *et al.*, 1978) but, more importantly, it permits for a physical interpretation of the factor $f_m(\omega)$: the polarizability per unit volume of the mth eigenmode.

APPENDIX B: DRUDE MODEL AND THE ELECTROSTATIC APPROXIMATION

According to the Drude model, the permittivity of a metal can be given by

$$\epsilon(\omega) = \epsilon_\infty^D - \frac{\omega_P^2}{\omega(\omega+i\Gamma_m)}. \tag{B1}$$

In order to get a closed analytical form of the factor f of Eq. (9), we consider the case when the frequency is close to a localized surface plasmon resonance $\omega = \omega_m + \delta$ and furthermore assume that $(\delta/\omega_m)^2 \ll 1$:

$$\begin{aligned}\epsilon(\omega) &= \epsilon_\infty^D - \frac{\omega_P^2}{(\omega_m+\delta)(\omega_m+\delta+i\Gamma_m)} \\ &\approx \epsilon_\infty^D - \frac{\omega_P^2}{\omega_m^2(1+2\delta/\omega_m+i\Gamma_m/\omega_m)}. \end{aligned} \tag{B2}$$

A Taylor expansion of the term in brackets in the denominator results in

$$\begin{aligned}\epsilon(\omega) &\approx \epsilon_\infty^D - \frac{\omega_P^2}{\omega_m^2(1+2\delta/\omega_m+i\Gamma_m/\omega_m)} \\ &\approx \epsilon_\infty^D - \frac{\omega_P^2}{\omega_m^2}\left(1-\frac{2\delta}{\omega_m}-\frac{i\Gamma_m}{\omega_m}\right) \\ &\approx \epsilon_\infty^D - \frac{\omega_P^2}{\omega_m^2} + \frac{2\omega_P^2}{\omega_m^3}(\omega-\omega_m+i\Gamma_m/2), \end{aligned} \tag{B3}$$

where we have kept only the first-order terms

With this result we now consider f:

$$f_m^j(\omega) \approx -\frac{2\epsilon_b^2(\gamma_m^j)^2}{(\gamma_m^j-1)^2}\frac{(\omega_m^j)^3}{\omega_P^2}\frac{1}{\omega-\omega_m^j+i\Gamma_m^j/2} = -\frac{A_m^j}{\omega-\omega_m^j+i\Gamma_m^j/2}, \tag{B4}$$

where Eq. (B2) has been used.

REFERENCES

Abasahl, B., C. Santschi, and O. Martin, 2014, ACS Photonics **1**, 403.

Ashcroft, N., and N. Mermin, 1976, *Solid State Physics* (Saunders College Publishing, Harcourt College Publishers, Sydney).

Barnes, W. L., A. Dereux, and T. W. Ebbesen, 2003, Nature (London) **424**, 824.

Bergman, D. J., 1978, Phys. Rep. **43**, 377.

Bergman, D. J., 1979a, J. Phys. C **12**, 4947.

Bergman, D. J., 1979b, Phys. Rev. B **19**, 2359.

Bergman, D. J., 1979c, J. Phys. C **12**, 4947.

Bergman, D. J., 1982, J. Phys. C **15**, 2033.

Bergman, D. J., and D. Stroud, 1992, Solid State Phys. **46**, 147.

Bohren, C., and D. Huffman, 1983, *Absorption and scattering of light by small particles* (John Wiley and Sons, New York).

Böttcher, C., O. van Belle, P. Bordewijk, and A. Rip, 1978, *Theory of electric polarization* (Elsevier Scientific Pub. Co., New York).

Bozhevolnyi, S. I., V. S. Volkov, E. Devaux, J.-Y. Laluet, and T. W. Ebbesen, 2006, Nature (London) **440**, 508.

Brandl, D. W., N. A. Mirin, and P. Nordlander, 2006, J. Phys. Chem. B **110**, 12302.

Carminati, R., J. Greffet, C. Henkel, and J. Vigoureux, 2006, Opt. Commun. **261**, 368.

Chang, D. E., A. S. Sorensen, P. R. Hemmer, and M. D. Lukin, 2006, Phys. Rev. Lett. **97**, 053002.

Cohen-Tannoudji, C., B. Diu, and F. Laloe, 1977, *Quantum Mechanics* (John Wiley and Sons, New York), Vol. 1.

Davis, T., K. Vernon, and D. Gómez, 2009, J. Appl. Phys. **106**, 043502.

Davis, T. J., and D. E. Gómez, 2014, Phys. Rev. B **90**, 235424.

Davis, T. J., D. E. Gómez, and F. Eftekhari, 2014, Opt. Lett. **39**, 4938.

Davis, T. J., D. E. Gómez, and K. C. Vernon, 2010a, Phys. Rev. B **82**, 205434.

Davis, T. J., D. E. Gómez, and K. C. Vernon, 2010b, Phys. Rev. B **81**, 045432.

Davis, T. J., D. E. Gómez, and K. C. Vernon, 2010c, Nano Lett. **10**, 2618.

Davis, T. J., and E. Hendry, 2013, Phys. Rev. B **87**, 085405.

Davis, T. J., M. Hentschel, N. Liu, and H. Giessen, 2012, ACS Nano **6**, 1291.

Davis, T. J., K. C. Vernon, and D. E. Gómez, 2009a, Phys. Rev. B **79**, 155423.

Davis, T. J., K. C. Vernon, and D. E. Gómez, 2009b, Opt. Express **17**, 23655.

Draine, B., and P. Flatau, 2003, arXiv:astro-ph/0309069.

Dregely, D., R. Taubert, J. Dorfmuller, R. Vogelgesang, K. Kern, and H. Giessen, 2011, Nat. Commun. **2**, 267.

Ebbesen, T. W., C. Genet, and S. I. Bozhevolnyi, 2008, Phys. Today **61**, 44.

Eftekhari, F., and T. Davis, 2012, Phys. Rev. B **86**, 075428.

Eftekhari, F., D. Gómez, and T. Davis, 2014, Opt. Lett. **39**, 2994.

Engheta, N., 2007, Science **317**, 1698.

Engheta, N., A. Salandrino, and A. Alù, 2005, Phys. Rev. Lett. **95**, 095504.

Fakonas, J. S., H. Lee, Y. A. Kelaita, and H. A. Atwater, 2014, Nat. Photonics **8**, 317.

Fano, U., 1961, Phys. Rev. **124**, 1866.

Funston, A., C. Novo, T. Davis, and P. Mulvaney, 2009, Nano Lett. **9**, 1651.

Gallinet, B., and O. J. F. Martin, 2011, Phys. Rev. B **83**, 235427.

Gallinet, B., T. Siegfried, H. Sigg, P. Nordlander, and O. J. F. Martin, 2013, Nano Lett. **13**, 497.

García de Abajo, F. J., and A. Howie, 2002, Phys. Rev. B **65**, 115418.

Gómez, D. E., A. Roberts, T. J. Davis, and K. C. Vernon, 2012, Phys. Rev. B **86**, 035411.

Gómez, D. E., Z.-Q. Teo, M. Altissimo, T. J. Davis, S. Earl, and A. Roberts, 2013, Nano Lett. **13**, 3722.

Gómez, D. E., K. C. Vernon, and T. J. Davis, 2010, Phys. Rev. B **81**, 075414.

Halas, N. J., S. Lal, W.-S. Chang, S. Link, and P. Nordlander, 2011, Chem. Rev. **111**, 3913.

Haynes, C., and R. P. Van Duyne, 2001, J. Phys. Chem. B **105**, 5599.

Hohenester, U., and J. Krenn, 2005, Phys. Rev. B **72**, 195429.

Hohenester, U., and A. Trugler, 2012, Comput. Phys. Commun. **183**, 370.

Hokari, R., Y. Kanamori, and K. Hane, 2014, J. Opt. Soc. Am. B **31**, 1000.

Jackson, J. D., 1975, *Classical Electrodynamics* (John Wiley & Sons Inc., New York), 2nd ed.

Jain, P., S. Eustis, and M. El-Sayed, 2006, J. Phys. Chem. B **110**, 18243.

Kantor, Y., and D. Bergman, 1982, J. Phys. C **15**, 2033.

Kellog, O. D., 1929, *Foundations of Potential Theory* (Frederick Ungar Publishing Co., New York).

Kim, T. J., T. Thio, T. W. Ebbesen, D. E. Grupp, and H. J. Lezec, 1999, Opt. Lett. **24**, 256.

Kittel, C., 1956, *Introduction to Solid State Physics* (Wiley, New York), 2nd ed.

Kosako, T., Y. Kadoya, and H. F. Hofmann, 2010, Nat. Photonics **4**, 312.

Kreibig, U., and M. Vollmer, 1995, *Optical Properties of Metal Clusters*, Springer Series in Materials Science Vol. 25 (Springer-Verlag, Berlin).

Lalanne, P., and M. P. Jurek, 1998, J. Mod. Opt. **45**, 1357.

Lalanne, P., and G. M. Morris, 1996, J. Opt. Soc. Am. A **13**, 779.

Langguth, L., A. H. Schokker, K. Guo, and A. F. Koenderink, 2015, Phys. Rev. B **92**, 205401.

Lezec, H. J., J. A. Dionne, and H. A. Atwater, 2007, Science **316**, 430.

Li, Z., S. Butun, and K. Aydin, 2014, ACS Nano **8**, 8242.

Liu, N., M. Hentschel, T. Weiss, A. P. Alivisatos, and H. Giessen, 2011, Science **332**, 1407.

Liu, N., L. Langguth, T. Weiss, J. Kastel, M. Fleischhauer, T. Pfau, and H. Giessen, 2009, Nat. Mater. **8**, 758.

Liu, N., F. Wen, Y. Zhao, Y. Wang, P. Nordlander, N. Halas, and A. Alù, 2013, Nano Lett. **13**, 142.

Liu, Z., J. M. Steele, W. Srituravanich, Y. Pikus, C. Sun, and X. Zhang, 2005, Nano Lett. **5**, 1726.

Lovera, A., B. Gallinet, P. Nordlander, and O. J. Martin, 2013, ACS Nano **7**, 4527.

Luk'yanchuk, B., N. I. Zheludev, S. A. Maier, N. J. Halas, P. Nordlander, H. Giessen, and C. T. Chong, 2010, Nat. Mater. **9**, 707.

Maier, S., 2007, *Plasmonics: Fundamentals and Applications* (Springer, New York).

Mäkitalo, J., M. Kauranen, and S. Suuriniemi, 2014, Phys. Rev. B **89**, 165429.
Mayergoyz, I. D., D. R. Fredkin, and Z. Zhang, 2005, Phys. Rev. B **72**, 155412.
Mayergoyz, I. D., Z. Zhang, and G. Miano, 2007, Phys. Rev. Lett. **98**, 147401.
Meystre, P., and M. Sargent, 1998, *Elements of Quantum Optics* (Springer, Berlin, Heidelberg).
Mie, G., 1908, Ann. Phys. (Berlin) **330**, 377.
Ming, T., L. Zhao, Z. Yang, H. Chen, L. Sun, J. Wang, and C. Yan, 2009, Nano Lett. **9**, 3896.
Mirin, N. A., K. Bao, and P. Nordlander, 2009, J. Phys. Chem. A **113**, 4028.
Miroshnichenko, A. E., S. Flach, and Y. S. Kivshar, 2010, Rev. Mod. Phys. **82**, 2257.
Moharam, M. G., T. K. Gaylord, E. B. Grann, and D. A. Pommet, 1995, J. Opt. Soc. Am. A **12**, 1068.
Mojarad, N. M., and M. Agio, 2009, Opt. Express **17**, 117.
Nordlander, P., C. Oubre, E. Prodan, K. Li, and M. Stockman, 2004, Nano Lett. **4**, 899.
Odom, T. W., and G. C. Schatz, 2011, Chem. Rev. **111**, 3667.
Ouyang, F., and M. Isaacson, 1989, Philos. Mag. B **60**, 481.
Ozbay, E., 2006, Science **311**, 189.
Pacifici, D., H. Lezec, and H. Atwater, 2007, Nat. Photonics **1**, 402.
Prodan, E., and P. Nordlander, 2004, J. Chem. Phys. **120**, 5444.
Prodan, E., C. Radloff, N. Halas, and P. Nordlander, 2003, Science **302**, 419.
Raether, H., 1977, in *Physics of Thin Films*, edited by G. Hass, M. H. Francombe, and R. W. Hoffman (Academic Press, New York), Vol. 9, pp. 145–261.
Raether, H., 1988, *Surface Plasmons on Smooth and Rough Surfaces and on Gratings*, Springer Tracts in Modern Physics (Springer, Berlin, Heidelberg).
Rechberger, W., A. Hohenau, A. Leitner, J. Krenn, B. Lamprecht, and F. Aussenegg, 2003, Opt. Commun. **220**, 137.
Sancho-Parramon, J., and S. Bosch, 2012, ACS Nano **6**, 8415.
Savage, K. J., M. M. Hawkeye, R. Esteban, A. G. Borisov, J. Aizpurua, and J. J. Baumberg, 2012, Nature (London) **491**, 574.
Schouten, H. F., N. Kuzmin, G. Dubois, T. D. Visser, G. Gbur, P. F. A. Alkemade, H. Blok, G. W. t. Hooft, D. Lenstra, and E. R. Eliel, 2005, Phys. Rev. Lett. **94**, 053901.
Sönnichsen, C., T. Franzl, T. Wilk, G. von Plesson, J. Feldmann, O. Wilson, and P. Mulvaney, 2002, Phys. Rev. Lett. **88**, 077402.
Su, K., Q. Wei, X. Zhang, J. Mock, D. Smith, and S. Schultz, 2003, Nano Lett. **3**, 1087.
Sun, Y., B. Edwards, A. Alu, and N. Engheta, 2012, Nat. Mater. **11**, 208.
Taflove, A., *et al.*, 2000, *Computational electrodynamics: The finite-difference time-domain method* (Artech House, Boston).
Taubert, R., M. Hentschel, J. Kästel, and H. Giessen, 2012, Nano Lett. **12**, 1367.
Thaxton, R., and C. Mirkin, 2005, Nat. Biotechnol. **23**, 681.
Vernon, K., A. Funston, C. Novo, D. Gómez, P. Mulvaney, and T. J. Davis, 2010, Nano Lett. **10**, 2080.
Weaver, J. H., and H. P. R. Frederikse, 2006, in *CRC Handbook of Chemistry and Physics* (CRC Press, Boca Raton, FL), 87th ed.
Wei, H., A. Reyes-Coronado, P. Nordlander, J. Aizpurua, and H. Xu, 2010, ACS Nano **4**, 2649.
Weiss, T., N. A. Gippius, S. G. Tikhodeev, G. Granet, and H. Giessen, 2009, J. Opt. A **11**, 114019.
Wokaun, A., J. P. Gordon, and P. F. Liao, 1982, Phys. Rev. Lett. **48**, 957.
Yang, S.-C., H. Kobori, C.-L. He, M.-H. Lin, H.-Y. Chen, C. Li, M. Kanehara, T. Teranishi, and S. Gwo, 2010, Nano Lett. **10**, 632.
Yurkin, M., and A. Hoekstra, 2007, J. Quant. Spectrosc. Radiat. Transfer **106**, 558.
Zayats, A., I. Smolyaninov, and A. Maradudin, 2005, Phys. Rep. **408**, 131.
Zhang, S., D. Genov, Y. Wang, M. Liu, and X. Zhang, 2008, Phys. Rev. Lett. **101**, 047401.
Zhu, W., R. Esteban, A. G. Borisov, J. J. Baumberg, P. Nordlander, H. J. Lezec, J. Aizpurua, and K. B. Crozier, 2016, Nat. Commun. **7**, 11495.